The Journal of Experimental Biology 210, 3644-3660
Published by The Company of Biologists 2007
doi:10.1242/jeb.008516

Sex and flow: the consequences of fluid shear for sperm–egg interactions

Jeffrey A. Riffell[1,*,†] and Richard K. Zimmer[1,2,†]

[1]*Department of Ecology and Evolutionary Biology and* [2]*Neurosciences Program and Brain Research Institute, University of California, Los Angeles, CA 90095-1606, USA*

*Author for correspondence at present address: ARL Division of Neurobiology, University of Arizona, Tucson, AZ 85721-0077, USA (e-mail: jeffr@neurobio.arizona.edu)

†Both authors contributed equally to this work

Accepted 17 August 2007

Summary

Fertilization is a complex interaction among biological traits of gametes and physical properties of the fluid environment. At the scale of fertilization (0.01–1 mm), sperm encounter eggs while being transported within a laminar (or viscous) shear flow. Varying laminar-shear in a Taylor-Couette flow tank, our experiments simulated important aspects of small-scale turbulence within the natural habitats of red abalone (*Haliotis rufescens*), a large marine mollusk and external fertilizer. Behavioral interactions between individual cells, sperm–egg encounter rates, and fertilization success were quantified, simultaneously, using a custom-built infrared laser and computer-assisted video imaging system. Relative to still water, sperm swam faster and moved towards an egg surface, but only in comparatively slow flows. Encounter rate, swim speed and orientation, and fertilization success each peaked at the lowest shear tested (0.1 s^{-1}), and then decayed as shear increased beyond 1.0 s^{-1}. The decay did not result, however, from damage to either sperm or eggs. Analytical and numerical models were used to estimate the propulsive force generated by sperm swimming (F_{swim}) and the shear force produced by fluid motion within the vicinity of a rotating egg (F_{shear}). To first order, male gametes were modeled as prolate spheroids. The ratio F_{swim}/F_{shear} was useful in explaining sperm–egg interactions. At low shears where $F_{swim}/F_{shear}>1$, sperm swam towards eggs, encounter rates were pronounced, and fertilization success was very high; behavior overpowered fluid motion. In contrast, sperm swimming, encounter rate and fertilization success all decayed rapidly when $F_{swim}/F_{shear}<1$; fluid motion dominated behavior. The shears maximizing fertilization success in the lab typically characterized natural flow microenvironments of spawning red abalone. Gamete behavior thus emerges as a critical determinant of sexual reproduction in the turbulent sea.

Supplementary material available online at
http://jeb.biologists.org/cgi/content/full/210/20/3644/DC1

Key words: fertilization, gamete interactions, shear, sperm behavior, turbulence.

Introduction

Traditionally, experimental studies of cell motility and locomotory behavior have been conducted in still water. These investigations have been valuable in determining the mechanisms governing cell movement (Engelmann, 1883; Gray and Hancock, 1955; Miller, 1979). As a consequence, much is known about the molecular basis of motility, including the mechanical principles that govern flagellar rotation and the expression of sensory-mediated behavior (Adler, 1969; Clarke and Koshland, 1979; Packer and Armitage, 1993). Most cells live, however, in a natural world of fluid motion. To appreciate fully the ecological context for behavior requires understanding the relationship between flow and cell motility. Where and when does behavior make a difference?

Fluid motion and single cells

Fluid motion is characterized by swirling turbulent eddies at relatively large spatial scales (1 mm–10 m; high Reynolds numbers) due to inertial forces, such as those generated by heat convection and muscular contractions (Goldsmith and Turitto, 1986; Chorin, 1994). Most single cells are smaller ($\ll$1 mm) than the tiniest of eddies (Banse, 1982; Jannasch et al., 1989; West et al., 1997). They also swim very slowly (<1 mm s^{-1}) or not at all, and thus, inhabit a microscopic setting (low Reynolds number) dominated by viscous forces (Berg and Purcell, 1977; Katz et al., 1981; Berg, 1983; Fulford et al., 1998). In this hydrodynamic regime, fluid particles tend to move as a unit. Adjacent layers of fluid slide past each other without being mixed. Much like a pot of honey stirred by a spoon, the fluid moves along streamlines and quickly stops when the action ceases. Within the smallest eddies, speed increases from the center towards the periphery, and therefore characterizes the laminar 'shear' flow (Hjelmfelt and Mokros, 1966; Tennekes and Lumley, 1972; Kundu, 1990). Single cells experience shear stress on the membrane surface as a consequence of fluid motion. The stress exists when cells are suspended in a moving

fluid, or are attached to a wall (e.g. a blood vessel or uterus) at any fluid–surface interface.

Despite an overwhelming focus on still water, the proportionately fewer studies in flow yield intriguing insights. Fluid-dynamics research provides excellent theoretical and empirical tools for examining the relationships between laminar-shear flow and cell behavior (Adler, 1981; Konstantopoulos et al., 1998; Chen et al., 2004). Specialized flow chambers, such as the Taylor-Couette apparatus (Bartok and Mason, 1957; Goldsmith and Marlow, 1972; Karp-Boss and Jumars, 1998; Ameer et al., 1999), cone-and-plate viscometer (Highgate and Whorlow, 1970; Solomon and Boger, 1998) and many types of microfabricated devices (Dellimore, 1976; Meng et al., 2005), have enabled studies of flow and particle interactions. Several results have shown that flow dominates behavior and cells are transported like passive particles (Rossman, 1937; Happel and Brenner, 1965; Shimeta et al., 1995; Karp-Boss et al., 2000; Dombrowski et al., 2004). Shear induced, for example, leukocyte tumbling under hydrodynamic conditions that typify the blood flow of mammalian arteries and veins (Cinamon et al., 2001; Goldsmith et al., 2001; Kadash et al., 2004). Such movements, although passive, would enhance contact rates between white blood cells and pathogenic bacteria (Brooks and Trust, 1983; Li et al., 2000; Thomas et al., 2002). Similarly, chains of single-celled plants (e.g. diatoms and cyanobacteria) bend, tumble or break in response to shear characterizing open ocean habitats (Karp-Boss and Jumars, 1998; O'Brien et al., 2004). Thinning the concentration boundary layers around cells, nutrient uptake would be enhanced *via* diffusion (Logan and Kirchman, 1991; Karp-Boss et al., 1996; Short et al., 2006). Even bacteria in water droplets are affected by shear. Over time, cells are concentrated at the air–water interface by a buoyancy-driven flow; microbe proximity to the atmosphere increases gas exchange rates (Dombrowski et al., 2004; Tuval et al., 2005). Whether suspended in a water droplet, turbulent sea or mammalian blood vessel, cells change naturally in structure (Edwards et al., 1989; Girard and Nerem, 1995; Zirbel et al., 2000), function (Cinamon et al., 2001; McCue et al., 2004) and distribution (over time and in space) due simply to the shear associated with fluid motion.

In contrast, behavior sometimes can make a difference. Shear stimulates cardiac epithelial cells and select species of pathogenic bacteria to swim/crawl actively upstream under environmentally realistic conditions (Dickinson et al., 1995; Dickinson et al., 1997; Chen et al., 2004; Thomas et al., 2002; Shiu et al., 2004; Meng et al., 2005). Moreover, neutrophils exhibit strong directional migration (i.e. chemotaxis) in response to a combined shear flow and attractant concentration gradient (Jeon et al., 2002). Given that shear naturally affects cell processes (e.g. DNA transcription and translation), it may constrain or conspire with behavior to mediate critical ecological interactions.

Fluid motion and sperm–egg interactions

Sexual reproduction is ironically one of the least understood of all fundamental biological processes (Vacquier, 1998). For most species, sperm and egg live in a world dominated by viscous forces and subjected to the physics of laminar-shear flows (Karp-Boss et al., 1996; Denny et al., 2002; Fauci and Dillon, 2006). Male and female gametes of both internal and external fertilizing animals ultimately make contact and fuse in such environments. The shears generated by fluid motion within a human reproductive tract are nearly equivalent in magnitude to those characterizing coastal ocean habitats (Rossman, 1937; Winet et al., 1984; Pennington, 1985; Eytan et al., 2001). Consequently, elucidating flow/behavior interactions for external-fertilizing marine invertebrates ('broadcast spawners') could provide valuable insights regarding similar processes for internal-fertilizing vertebrates.

Notwithstanding the substantial research on cell motility, there is little mechanistic understanding of how flow affects sperm–egg interactions, male–female gamete encounter rates and, ultimately, fertilization success. Laminar-shear flow may promote fertilization by causing gametes to tumble and contact one other (Rothschild and Osborn, 1988; Denny et al., 1992). In contrast, fertilization might be limited if shear prevents sperm from attaching to the egg plasma membrane and/or vitelline envelope (or zona pellucida) (Shimeta and Jumars, 1991; Mead and Denny, 1995; Karp-Boss and Jumars, 1998). To date, only one study has examined the relationship between shear and fertilization success (Mead and Denny, 1995). A strong inhibitory effect of high shear ($>10\ s^{-1}$) on sea urchin fertilization was attributed to shear-induced gamete damage, but there were no direct observations of gamete interactions.

For red abalone, the present study provided direct measurements of sperm swimming (speed, near-instantaneous direction of travel), egg rotation rates, gamete encounters and fertilization as a function of laminar-shear. It established the shears that constrain and those that conspire with sperm behavior to either inhibit or promote fertilization, respectively. Sperm performed best and fertilization success was maximized under experimental conditions most closely simulating the hydrodynamics of adult natural habitats. Thus, shear may act as a decisive selective pressure driving the evolution of gamete behavior within native environments.

Materials and methods

Study animal and natural history

The red abalone *Haliotis rufescens* Swainson 1822 is a valuable species for studying the relationship between hydrodynamics and fertilization. As a large marine mollusk and external fertilizer, individual, mature males and females are found gravid year-round. They are induced to spawn in the laboratory on command (Morse et al., 1977; Ebert, 1992; Leighton, 2000), and a single gravid male or female releases about 10 billion sperm or 3 million eggs, respectively (Mottet, 1978; Leighton, 1989; Leighton, 2000). Consequently, profuse gamete material is available for experiments at almost all times. Juvenile and adult red abalone inhabit rocky reefs within giant kelp forests along the California coast (Fig. 1). Historically, adult males and females lived together in dense aggregations (Cox, 1962; Tutschulte, 1976). Recent demises due to human fishing and disease have greatly reduced wild population sizes, and therefore individuals are now often found as isolated (Davis et al., 1992; Daniels and Floren, 1998; Tegner, 2000). The animals feed primarily on dead kelp material, transported as

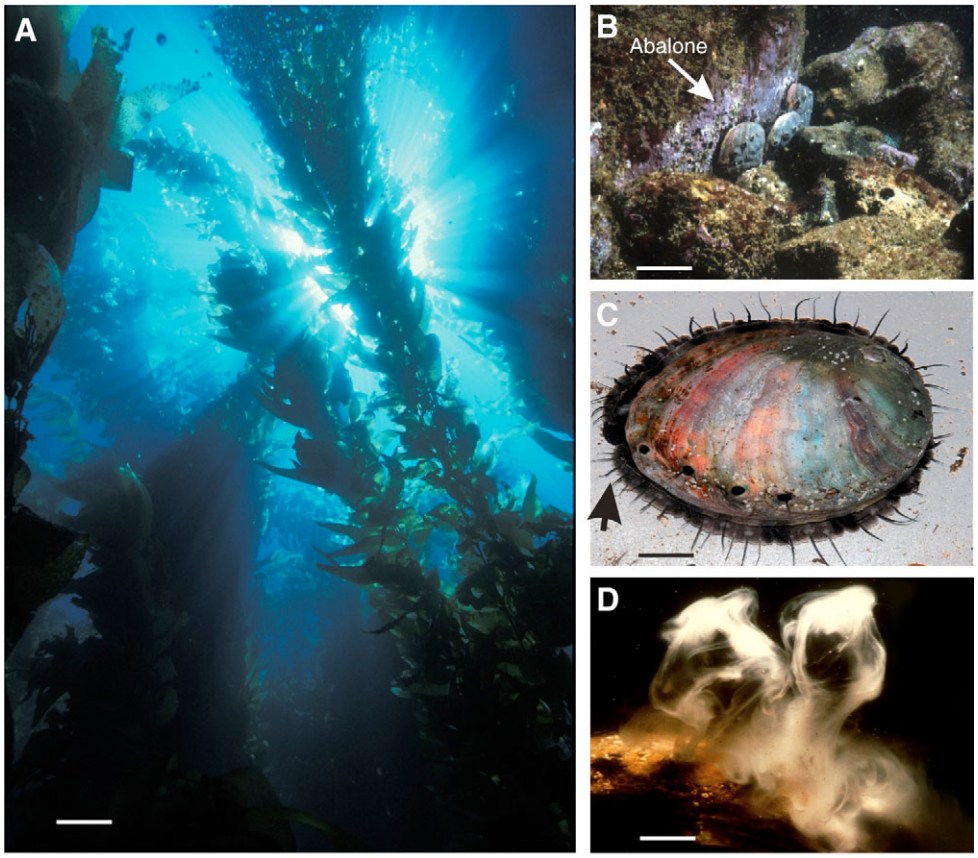

Fig. 1. (A). Open habitat of giant kelp forest in shallow (10–15 m depth), coastal waters offshore of Point Loma, San Diego, California (photo credit: Eric Hanauer). Bar, 25 cm. (B) Within this forest, adult red abalone aggregate underneath ledges and in crevices among rocky reefs. Hydrodynamic measurements characterized the physical properties of adult microhabitats and the open forest environment (photo credit: Eric Hanauer). Bar, 15 cm. (C) Each adult male or female spawns gametes into the sea *via* excurrent tremata, small holes in the shell that connect the mantle cavity (exit site for reproductive products) and surrounding ocean. The epipodium (lateral lobe of the foot) contains many small tentacles that are used in sensing water motion; two large cephalic tentacles (not shown) protrude from the head (to the left, arrow) and function primarily in olfaction (photo credit: L. Ignacio Vilchis). Bar, 1.0 cm. (D) Spawning of sperm by a single adult male. Propulsive forces generated by the muscular contractions of its foot ultimately produce a gamete jet, or plume (photo credit: Larry Friesen). Bar, 0.5 cm.

'drift' along the ocean floor by locally generated currents (Tutshulte and Connell, 1988; Leighton, 2000; Vilchis et al., 2005). On rocky reefs, red abalone live within cracks and crevices, or underneath ledges (Fig. 1) (Tutshulte, 1976; Tegner, 1989). It is thus within these unique microenvironments that gravid adults naturally spawn.

Field setting and flow environment

Field measurements within giant kelp forests (*Macrocystis pyrifera*) were designed to characterize the mixing properties of fluid into which abalone spawn, and to provide a regional context for these localized flows. These measurements specified the range of fluid-dynamic conditions for testing in laboratory flow tanks. Sites were chosen that historically supported large red abalone populations at Point Loma (San Diego, CA, USA; 32°67′N, 117°23′W) and Harris Point (San Miguel Island, CA, USA; 34°06′N, 120°36′W). Field work at Point Loma was performed over 12 days in May–December (1998–2000). The full range of tides, from spring to neap, occurred in approximately equal numbers. Variation in flow parameters was assessed from data taken over a range of significant wave heights (0.2–1.5 m) (Buoy 09101, 183 m depth, located directly offshore of the Point Loma kelp forest; Coastal Data Information Program, Scripps Institution of Oceanography, UC San Diego, CA, USA). The timing of SCUBA dives (and flow measurements) matched the period over which red abalone naturally spawn (Young and DeMartini, 1970). Harris Point was intended only as a comparison site, and here, field surveys were limited to 3 days in November, 1998.

Using SCUBA, red abalone density was censused over a series of 30 m long × 2 m wide band transects haphazardly selected at kelp forest locations of 10–20 m depth. Although mean abalone densities along transects varied from 0–0.76 individuals m^{-2} at each field location, aggregations of 3–7 adults m^{-2} were found at local 'hot spots' within crevices and particularly under ledges of rocky reefs. Flow speeds were measured at these hot spots using an acoustic Doppler velocimeter (SonTek Corp., San Diego, CA, USA) firmly mounted on the articulating arm of a stable tripod. The small size and sample volume (0.1 cm^3) of our custom-built Doppler probe allowed high-speed (30 Hz) measurements ~5 cm above abalone living in crevices and under ledges, and in adjacent open areas several meters away from rocky reefs and boulders. Continuous measurements were made over a 5–10 min interval (9000–18 000 ADV recordings) at each location, with sampling alternated between abalone microhabitat and paired open field sites (N=12 pairs; 24 total recordings). Three-dimensional velocity time series were then constructed for each 1 min interval (1800 ADV recordings). From these records, Reynolds stresses, turbulent energy dissipation rates and shears were estimated using established procedures (Hinze, 1975; Heathershaw and Simpson, 1978; Gross and Nowell, 1983; Kundu, 1990), after removing contributions of oscillatory motion due to surface waves (Trowbridge, 1998).

Taylor-Couette apparatus

At the scale of fertilization (0.01–1 mm; $Re \ll 1$), sperm encounter eggs while being transported within a sheared

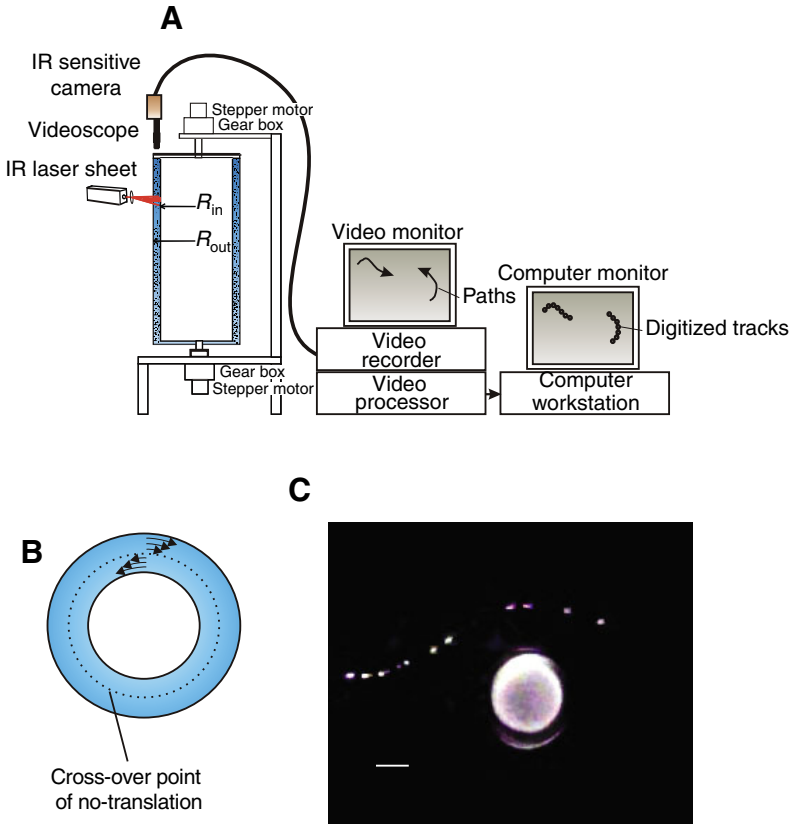

Fig. 2. (A) Side-view of the experimental set-up for imaging sperm-egg interactions (not drawn to scale). Here, the Taylor-Couette apparatus is mounted vertically for use in fertilization experiments. It consists of two nested cylinders, with an 8 mm wide seawater-filled gap between them. R_{in} and R_{out} refer to the radii of the inside (6.1 cm) and outside (6.9 cm) cylinders, respectively. Counter-rotation of the two cylinders produces a steady laminar flow over a wide range of shears (0–10 s^{-1}) at low Reynolds numbers (Re<150). Further details are provided in the text. (B) Top view of the seawater gap between vertically mounted cylinders with arrows denoting flow velocity vectors. A cross-over point of no translational velocity occurs between the counter-rotating flows. (C) A sequence of overlaid, digitized images (at 0.1 s intervals) of a single sperm, as it slips past an egg at 2 s^{-1}. The egg is positioned at the cross-over point, and thus remains stationary, while rotating from right to left. Bar, 100 μm.

(velocity gradient) viscous flow. This fluid-dynamic regime occurs inside the smallest eddies, where fluid motion is dominated by viscosity. Encounters between gametes were observed and fertilization rates quantified under conditions of laminar-shear flows in a Taylor-Couette apparatus [see details of theory and construction in Karp-Boss and Jumars (Karp-Boss and Jumars, 1998)]. This flow tank consists of two coaxial cylinders (20 cm tall, 6.1 and 6.9 cm radii) that rotate in opposite directions (Fig. 2). Seawater (0.22 μm-filtered) fills the 0.8 cm gap between the inner and outer cylinders. Because the sheared fluid associated with each cylinder moves in opposite directions, there is a predictable cross-over point of no translational velocity about midway through the fluid-filled gap (Trevalyan and Mason, 1951). The precise location of this cross-over point ($R_{stationary}$) is calculated as:

$$R_{stationary} = \left(\frac{R_{out}^2 R_{in}^2 (\Omega_{out} + \Omega_{in})}{R_{out}^2 \Omega_{out} + R_{in}^2 \Omega_{in}} \right)^{1/2}, \quad (1)$$

and shear, G (s^{-1}), at any point across the gap, is determined as:

$$G(R) = \frac{2(\Omega_{out} + \Omega_{in}) R_{out}^2 R_{in}^2}{R(R_{out}^2 - R_{in}^2)}. \quad (2)$$

Here, R_{in} and R_{out} are the radii of the inner and outer cylinders, and Ω_{in} and Ω_{out} are the angular velocities of the inner and outer cylinders, respectively. From Eqn 1 and Eqn 2, it follows that shear varies predictably across the fluid-filled gap. This change in shear is, however, negligible (<3%) over the small radius (100 μm) of an egg. Reported values of shear were calculated at the cross-over point of no translational velocity.

Abalone collection, maintenance and spawning

Each experiment was conducted using only fresh eggs and sperm (defined as 10–30 min post-spawn). Adult males and females were procured from The Cultured Abalone, Inc. (Goleta, CA, USA), or collected at field sites, and then held in aquaria of running seawater (15°C). The animals were fed fresh kelp *Macrocystis pyrifera*, collected twice weekly. Ripe adults were identified by gonadal growth beyond the shell (Hahn, 1989), and sexes were separated and fed for 2 weeks prior to spawning induction. Individuals were placed singly in chambers and the seawater pH raised to 9 by adding 6.5 ml of 2 mol l^{-1} tris-hydroxymethylaminomethane (Tris-base) per liter, followed by 4 ml of 6% H_2O_2 per liter (Morse et al., 1977). After 2.5 h exposure, the chamber was emptied, rinsed and refilled with 0.45 μm filtered seawater (FSW). Spawning occurred within 2–4 h of H_2O_2 exposure. Gametes were harvested above the excurrent tremata and held in centrifuge tubes (sperm) or beakers (eggs) filled with FSW until use.

Effects of fluid shear on fertilization success

The relationship between fluid shear and fertilization success was determined in the Taylor-Couette apparatus, filled with seawater and sperm at a concentration of 10^4, 10^5 or 10^6 cells ml^{-1}. A computer-controlled stepper motor system was activated after all visible air bubbles had been purged from the tank. Within 5 s, this unit brought the spinning cylinders to a designated shear of either 0.1, 0.5, 1.0, 2.0, 4.0 or 10.0 s^{-1}. Fifteen replicate trials were performed for each sperm concentration/shear treatment. Evaluation of several different egg-addition techniques *via* dye visualization yielded the following procedure. Immediately after the programmed shear was achieved, an egg suspension was introduced through a small portal at the top of the apparatus. 3 ml of an egg solution (10^5 cells ml^{-1}) were transferred slowly (over 10 s) into the middle of the seawater-filled gap, using a serotological pipette. The narrow, drawn-out pipette tip (3 mm i.d.) was placed 0.5 cm below the water surface during egg delivery. As indicated by

dye, flow disturbances were localized (within 1 cm of the water surface) and short lived (laminar flow permeated the apparatus within 1–2 s after pipette withdrawal).

Shear effects on fertilization were quantified for a single contact time. 15 s after egg introduction, 10 ml of mixed gamete suspension were withdrawn from the middle of the gap, 4 cm below the water surface. This time reflected a short, but realistic, gamete encounter interval in field habitats (Pennington, 1985; Levitan, 1998; Babcock and Keesing, 1999). The eggs (at ~10^3 ml^{-1}) were captured from suspension on a 100 μm mesh screen, and then rinsed thoroughly with 50 ml of FSW. Repeated microscopic examinations indicated that the rinse eliminated all sperm from egg surfaces, except those attached to the vitelline envelope. After 3 h incubation in FSW, eggs were fixed in 5% buffered formalin and assessed for percentage fertilized.

For comparison, trials were also performed in still water. The Taylor-Couette apparatus was again filled with seawater and sperm at a concentration of 10^4, 10^5 or 10^6 cells ml^{-1}, but the stepper motor system was not activated. In each trial, 1 ml of egg suspension (at 10^3 ml^{-1}) was pipetted gently into a clear plastic tube (4 cm long, 1 cm i.d.), with the sides and base (lower third) replaced with 150 μm mesh screen. The tube (with eggs) was clamped to a micromanipulator, and then lowered slowly (over 10 s) into a sperm solution. After 15 s, each tube was raised out of solution, eggs rinsed over 100 μm mesh, and fertilization censused as described above. A total of 15 replicate trials was performed for each sperm treatment. Using these methods, sperm–egg interactions were permitted in a three-dimensional environment with only minimal flow ($\leqslant$15 μm s^{-1}) due to convection (as determined by computer-assisted video motion analysis of dead sperm paths; see Materials and methods: measurements of sperm swimming speed and direction in shear flows). Computer-video imaging confirmed that sperm swim speeds and directions were unaffected by the mesh (data not shown). Filament thickness (33 μm) was inconsequential when compared to the size of open mesh.

Effects of fluid shear on sperm behavior and sperm–egg encounter rates

Subsequent research focused on the mechanisms by which fluid shear acts on sperm–egg interactions. In still water, abalone sperm orient to an egg-derived chemical attractant (Riffell et al., 2002; Riffell et al., 2004). New experiments were therefore performed to evaluate these behavioral interactions in laminar-shear flows.

Experimental procedures were identical to those already described (see Materials and methods: Effects of fluid shear on fertilization success), except for a few important differences. The Taylor-Couette apparatus was filled simultaneously with FSW, sperm (10^6 cells ml^{-1}) and eggs (10^2 cells ml^{-1}). In preliminary trials, these specific gamete concentrations promoted video imaging of sperm–egg interactions, while minimizing egg–egg collisions. All visible air bubbles were purged from the flow tank over 60 s. Then, the apparatus was tilted 90°, so its principal axis (20 cm length) lay horizontal. Male and female gametes were dispersed evenly throughout the fluid-filled gap over the entire length of the tank. Next, the spinning cylinders were activated by a computer-controlled stepper motor assembly, and flow was brought quickly (within 5 s) to a designated shear (0.1, 0.5, 1.0, 2.0, 4.0 or 10.0 s^{-1}). Horizontal orientation of the tank had no effect on fluid motion, but enabled suspension of sperm and eggs for 5–10 min with minimal loss due to gravitational sinking. Eight replicate trials were performed for each shear treatment. Although each trial ran for 5 min, video recordings were made only during the last 60 s. The rest of this time was used for focusing optics on eggs and sperm within a thin laser sheet (see Materials and methods: Instrumentation and computer-assisted video motion analysis).

As a control, each experimental treatment was repeated, except that brine shrimp eggs were substituted for their abalone counterparts. Brine shrimp eggs were excellent physical mimics, being essentially the same mean density (1.10±0.04 g ml^{-1}, mean ± s.e.m.) and radius (112±6 μm, mean ± s.e.m.) as abalone eggs (1.09±0.02 g ml^{-1}; 108±5 μm). Additional controls were performed using abalone eggs and dead sperm (with flagella intact), in order to compare results of replicated trials between treatment types. From these comparisons, the relative contributions could be determined of passive physical processes and of behavioral responses of live sperm to gamete encounter rates. Finally, a parallel set of experiments was performed identically in still water using mesh tubes with live or dead abalone sperm, and either abalone or brine shrimp eggs, as described above (see Materials and methods: Effects of fluid shear on fertilization success).

Instrumentation and computer-assisted video motion analysis

Within the Taylor-Couette apparatus, sperm–egg interactions were video imaged at the cross-over point of no translational velocity. Here, individual eggs remained stationary for 20–30 s at a time. The cells were illuminated with a narrow, focused light sheet (1 mm thick), using a low-energy, infrared (IR, 830 nm, 25 mW) laser diode (Coherent model NT54-029, Moorpark, CA, USA), equipped with a concave line-generating lens. This laser sheet lit an observation area along the plane of shear (i.e. the horizontal plane). Images were recorded by an IR-sensitive video camera (COHU Model 6415-2000, with active heads; San Diego, CA, USA) interfaced with a custom-built, long-range, video-microscope (Titan Tool Supply Co., Buffalo, NY, USA). Magnification was 47×, and the camera was oriented 90° to the axis of the laser sheet. The microscope focused on images at a point, 5.5 cm below the water surface, thus avoiding gamete interactions with the chamber walls.

Once captured, video images were processed using a computer-assisted video motion analyzer (Motion Analysis Corp. model VP 320, ExpertVision, Santa Rosa, CA, USA, and custom software) interfaced with a Sun SPARC 2 computer workstation (Gee and Zimmer-Faust, 1997). This system constructed a digitized record from raw analog data, using a gray scale detector to enhance the contrast between each object (i.e. gamete) in the video field and background. Each sperm head was outlined, and x,y coordinates of the centroid (geometrical center) were calculated. The path of a gamete (head) was reconstructed, on a frame-by-frame basis, as the translational movement through space of its centroids. To avoid mistaking vertically for horizontally moving gametes, we discarded short paths that consisted of computer images with cells changing more then 20% in apparent size. All paths that could be followed for at least six frames were included in the analysis.

Measurements of sperm swimming speed and direction in shear flows

The timing and precise location of each encounter between sperm and egg was recorded from digital images. Swim speed and direction of each sperm cell also were determined, within a 200 μm radius surrounding an egg. To eliminate effects of flow on measurements of swim speed, heat-killed sperm (20 min exposure at 40°C) were substituted for their live counterparts, and the measurements repeated (N=8 replicate trials for each shear). The dead sperm served as passive particles, revealing the background fluid movement experienced by live gametes. From paths of dead sperm, two-dimensional velocity fields were mapped with respect to positions (x,y coordinates) within the gap. The computed velocities based on dead sperm paths were then subtracted from live sperm paths on a frame-by-frame basis, using a customized MATLAB program.

Elimination of the flow component from a live cell path revealed the direction of swimming within a circular coordinate system. Here, θ is the angle relative to an operationally defined origin (0°) and **r** is the unit vector (Batschelet, 1981) for $i…n$ cells in a population:

$$\mathbf{r} = \left\{ \frac{1}{n} \left[\left(\sum \cos\theta_i \right)^2 + \left(\sum \sin\theta_i \right)^2 \right] \right\}^{1/2} . \quad (3)$$

A unit vector length of 1 indicates that all sperm swam on a single trajectory for a given treatment. In contrast, a length of zero denotes random movements without a shared bearing. Two questions were evaluated: did cells orient relative to flow or egg surface? According to the first, cells swimming in straight paths, upstream or downstream, would move with θ of 0° or 180°, respectively. The coordinate system was set up with the origin facing directly into flow. According to the second, sperm swimming trajectory was evaluated with respect to the nearest egg. In this case, the origin was defined as the tangent between each cell and the center of the egg. Sperm moving directly towards an egg thus would follow a 0° heading. For each treatment, these two separate analyses were performed on the same data set. A Rayleigh's test was applied initially to compare the mean direction swum against a uniform circular distribution. If significantly different, a V-test was used to determine the fit with respect to each of the origins.

Effects of fluid shear on gamete morphology and viability

Sperm morphology and swim speed

In addition to gamete motion, fluid shears can have other significant effects that impact fertilization. High shears are known, for example, to damage flagella mechanically and impair their motility. To investigate this possibility, red abalone sperm (at 10^6 cells ml^{-1}) were sheared (0, 0.1, 0.5, 1.0, 2.0, 4.0 and 10.0 s^{-1}) for 60 s in the absence of eggs. Identical procedures were employed as described above. Three replicate trails were conducted for each shear treatment. Both before and after shearing, triplicate samples (200 μl) of sperm suspensions were withdrawn from the Taylor-Couette apparatus. Each sample was placed in a separate hemocytometer, and mounted on an Olympus IX70 compound light microscope at 90× magnification. The percentages of flagella retaining their natural size (20–25 μm) and motility were determined for the first 100 sperm encountered in each sample.

Swim paths were quantified in a second set of triplicate samples from each sperm suspension, before and again after shearing. Each sperm sample was put in a separate Plexiglas™ chamber (10 mm×10 mm×5 mm length×width×depth) and diluted with filtered seawater to 10^3 cells ml^{-1}. Images of sperm swimming were recorded on magnetic tape over 60 s using a video camera (NEC model TI 23A, Tokyo, Japan) as attached to the compound microscope. The camera had a 100 μm depth of field and focused on a region approximately 2 mm (70 sperm body lengths), away from the nearest chamber wall. Swimming speeds of individual cells were determined using computer-assisted video motion analysis (see Materials and methods: Effects of fluid shear on sperm behavior and sperm–egg encounter rates). A minimum of 25 swimming paths were analyzed for each treatment.

Egg morphology

Fluid shear might damage egg membranes, or erode the jelly coat, thereby reducing fertilization success. To examine these possible effects, the above experiments were repeated, but eggs were sheared (0, 0.1, 0.5, 1.0, 2.0, 4.0 and 10.0 s^{-1}) for 60 s without sperm present. Three replicate trials were conducted of each shear treatment. Before and after shearing, triplicate samples of egg suspensions (2 ml) were removed from the Taylor-Couette flow tank and viewed through a compound microscope. For the first 100 eggs from each sample, the egg membrane and jelly coat were inspected for visible damage. The diameters of 10 eggs per shear treatment were measured from photomicrographs, after addition of Sumi ink to visualize the jelly coat. A significant decrease in diameter after shearing could indicate a loss of jelly and/or cytoplasm.

Proclivity for fertilization

Gamete inclination for fertilization may be affected adversely by high fluid shear in other unidentified ways. For this reason, we performed two additional series of trials. In the first, four samples of sperm were collected before and after 60 s of shearing (0, 0.1, 0.5, 1.0, 2.0, 4.0 and 10.0 s^{-1}). Each sample was then combined with fresh (never-been-sheared) eggs in a separate Plexiglas™ chamber (3.0 ml volume). Following dilution with seawater, final chamber concentrations were 10^6 sperm ml^{-1} and 10^2 eggs ml^{-1}. The eggs in each chamber were removed after 1 min, rinsed thoroughly with 50 ml FSW, incubated for 3 h, fixed in 5% buffered formalin, and assessed for percentage fertilization. A second series of trials was performed identically to the first, but using sheared eggs and fresh sperm. For each trial series, significant differences in percentages of fertilized eggs would be expected between 'before' and 'after' treatments, if shearing affected gamete performance.

Theoretical considerations

Propulsive and shear forces

There is a threshold above which relatively high shear overcomes sperm swimming. To estimate this threshold (F_{swim}/F_{shear}=1), analytical models were used to determine both the propulsive force generated by a sperm swimming (F_{swim}) and the shear force produced by fluid motion within the vicinity

of a rotating egg (F_{shear}). Here, we modeled sperm as prolate spheroids, a geometry conforming well to cell body shape minus the flagellum. The propulsive force during steady swimming was calculated as:

$$F_{swim} = \mu \left(\frac{4\pi l}{\ln(2l/d) - \frac{1}{2}} \right) u \,, \quad (4)$$

where μ is the dynamic viscosity of seawater (1.2×10^{-3} N s m^{-2}), l is the length of the sperm body, d is the width of the cell, and u is the swimming speed (Berg, 1983). Shear force was computed by multiplying the laminar-shear stress (of the velocity gradient) times the cell surface area:

$$F_{shear} = c\mu \frac{\partial u}{\partial y} \,, \quad (5)$$

where $(\partial u/\partial y)$ is the shear, and c is the average surface area of a sperm (a prolate spheroid=6.8×10^{-10} m^2).

To first order, these computations of propulsive and shear forces provided a reasonable facsimile of nature. The surface area of the cell body of an abalone sperm is 4.25-times larger than that of a flagellum. Moreover, the cell body is exposed to significantly higher shears than a flagellum, as swimming sperm approach a rotating egg. Consequently, a flagellum makes only a small contribution to overall drag and shear stress. To our knowledge, no one has established computationally the relationship between laminar shear flow and flagellum performance. Such investigation would require precise time-dependent information on complex, flagellar waveform mechanics and force-generation mechanisms (e.g. molecular motors driving the flagellum), well beyond the scope of the current study.

Gamete rotation

The shear generated by a Taylor-Couette flow causes particles to rotate. When transported passively, spherical eggs are predicted to spin at a constant rate while sperm (as spherical prolates) should align with flow streamlines and 'flip' (or 'rotate') periodically (Bartok and Mason, 1957; Karp-Boss and Jumars, 1998). Gamete rotation rates at each tested shear were measured and compared to theoretical predictions for spheres (eggs) and prolate spheroids (sperm) immersed in a sheared fluid (Jeffrey, 1922):

$$0.5T = \frac{2\pi}{G} \left(r_a + \frac{1}{r_a} \right), \quad (6)$$

where r_a is the axis ratio (length/width) of the gamete (e.g. r_a=1 for the egg), and T is the period of gamete rotation. For each shear treatment, rotation rates were measured for 10 sperm and 10 eggs as selected from a random numbers table. According to theory (Jeffrey, 1922), non-motile eggs and dead sperm always rotate at predicted rates, regardless of shear magnitude. In contrast, paths of live sperm should change substantially as a function of shear. The threshold thus acts as an inflection point; live sperm are predicted to rotate, end-over-end, only at higher shears.

Flow fields around eggs

Ambient fluid motion could cause sperm and eggs to tumble into contact with each other. Then again, sperm may be physically prevented from attaching to the egg surface at some limiting (high) shear value. To evaluate these alternative scenarios, we described the flow fields and shear stresses at varying points in space surrounding a rotating egg. Irrespective of sperm swimming speed and direction, hydrodynamic-induced motions of gametes might enhance or retard their encounter rates, depending on the magnitude of fluid shear. In fact, sperm navigation is complex. Fluid at the surface of an egg moves at the instantaneous velocity (v_Ω) of a rotating sphere, as a consequence of laminar-shear flow:

$$v_\Omega = 2\pi r / T \,, \quad (7)$$

where r is egg radius. This rotation locally thins the boundary layer and increases the shear stress near the egg surface. Moreover, rotation creates an asymmetry in the distribution of shear stress, with higher pressure on the egg surface facing into flow. Thus, we determined the magnitudes of shear forces acting on sperm at different points within each flow field. The Navier–Stokes equation for creeping flow is:

$$\rho \frac{\partial u}{\partial t} + \rho u \nabla u = \mu \nabla^2 u - \nabla p + C \,, \quad (8)$$

where ρ is seawater density, p is pressure, C is a constant, and ∇ indicates partial derivatives in all three spatial dimensions (e.g. $\partial/\partial x+\partial/\partial y+\partial/\partial z$). To model the flow field around a rotating egg, Eqn 7 and Eqn 8 were coupled using custom FEMLAB (v. 3.3, Comsol, Inc., Los Angeles, CA, USA) and MATLAB (v. 7.02, MathWorks, Inc., Natick, MA, USA) programs, and solved numerically using the finite element method (Verfürth, 1996; Zimmerman, 2004; Pepper and Heinrich, 2005). The selected element size (4×10^{-12} m^2) defined flow fields and shear stresses (and forces) at high resolution within <1 μm of an egg surface. Sensitivity analysis showed that the chosen domain size of 1000r generated <1% error in model outputs.

Results

Field setting and flow environment

This study focused on fertilization processes occurring within centimeters of substrate occupied by abalone. Given that mixing within the flow microhabitats did, to some extent, depend on the specific geometries of crevices and ledges, as well as on upstream conditions, the field measurements are illustrative only. Steady, longshore currents were exceedingly weak, but cross-shelf currents were strong in open habitats of kelp forests (Table 1). Water flow speeds among rocky ledges and crevices harboring red abalone ('hot spots') were 2–3 times slower than in exposed areas. These hot spots exhibited significantly smaller Reynolds stresses, turbulent energy dissipation rates, and shears (Table 1 and Fig. 3). Overall, shears ranged from 0.3–2.4 s^{-1} and 4.8–13.4 s^{-1} in hot spots and open habitats, respectively. Moreover, energy dissipation rates of hot spots were similar to those measured in the surface mixed layer of the open ocean [e.g. 10^{-1} cm^2 s^{-3} (Gargett, 1989)], as opposed to the very strong turbulence measured in coastal tidal channels [e.g. 10^2 cm^2 s^{-3} (Wesson and Gregg, 1994)]. Thus, red abalone aggregated at sites where water motion was substantially retarded.

Table 1. *Properties of near-bottom flows in open kelp forest and red abalone microhabitats, offshore of Point Loma, San Diego, California, USA*

	Open			Crevices and ledges		
Variable	Median	10%	90%	Median	10%	90%
Dissipation rate, ϵ ($cm^2\ s^{-3}$)	1.91	0.54	4.26	0.024*	0.003	0.159
Shear, G (s^{-1})	8.95	4.76	13.37	0.79*	0.33	2.37
Reynolds stress, τ ($N\ s^{-1}$)	0.45	0.086	3.82	0.089*	0.007	0.46
Wave period (s)	10.7	8.7	13.03	NA	NA	NA
Flow speed, U ($cm\ s^{-1}$)	9.62	6.03	17.91	5.22*	2.97	7.70

*P<0.0001; asterisk denotes a significant difference between open and crevices/ledges sites (one-way ANOVA: $F_{1,102}$>25.71, all comparisons). NA=not applicable.

Effects of fluid shear on fertilization success

Fertilization success was either promoted or inhibited, depending on the magnitude of fluid shear. Similar patterns emerged across all sperm treatments. The percentage of fertilized eggs peaked at 0.1 s^{-1}, and then decayed as a function of increasing shear (Fig. 4). At sperm concentrations of 10^5 and 10^4 cells ml^{-1}, maximal percentages of fertilized eggs were about 1.5 times those measured in still water. In contrast, the maximal value declined (1.2 times) slightly at a higher sperm density (10^6 cells ml^{-1}), as overall fertilization levels approached an asymptote of 100%. Compared to still water, fertilization success was significantly elevated at shears of 0.1–1.0 s^{-1} (ANOVA and Scheffé tests: P<0.0001; see supplementary material Table S1), was the same at 2.0 s^{-1}, and was significantly reduced at 4.0 and 10.0 s^{-1} (Fig. 4; Scheffé test, P<0.05).

Characterization of fluid shear in the Taylor-Couette apparatus

The Taylor-Couette apparatus reliably generated well-behaved laminar-shear flows. Velocity fields were mapped across the seawater-filled gap of the Taylor-Couette apparatus, using ~600 dead sperm as passive tracers for quantitative flow visualizations. Taking the cross-over point ($R_{stationary}$) of no translational velocity as the origin (y=0), flow speed increased linearly as a function of distance across the gap (Fig. 5A). Little variation between measurements was found in replicate trials for any given set of experimental conditions (Fig. 5B). Calculations of shear were made according to theory (see Eqn 2), and based on empirical determinations. Comparisons between predicted and empirical results for each replicate showed excellent agreement over all shear treatments (0.1, 0.5, 1.0, 2.0, 4.0 and 10.0 s^{-1}; Fig. 5B). Hence, the computer/video imaging system provided accurate, high-resolution measurements of particle velocities.

Effects of fluid shear on sperm swimming and sperm–egg encounter rates

Male gamete behavior could predict fertilization success. As a function of fluid shear, sperm swim speed and orientation (relative to an abalone egg), gamete encounter rate and percentage of fertilized eggs, all were significantly correlated (Table 2 and Figs 4, 6, and 7; Pearson's product moment correlation: r^2>0.82, d.f.=6, P<0.05, all comparisons). Sperm swam faster in the presence of and moved towards an abalone

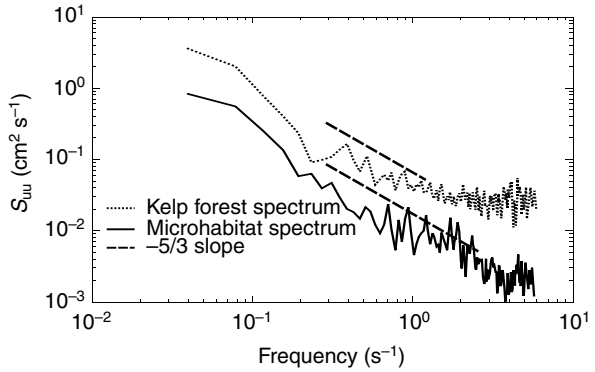

Fig. 3. Two representative spectra (with wave energy subtracted) describing the relationship between power, S_{uu} (y axis), and frequency (x axis) of turbulent fluctuations in flow speed along a principal axis. Measurements were taken within a microhabitat harboring abalone (solid line), and 3 m away on the seafloor of an open kelp forest (dotted line). Energy dissipation rates and fluid shears were estimated from the spectral intensities of the inertial subrange (i.e. where the spectra exhibit the –5/3 slope; broken lines), following published methods (Hinze, 1975; Trowbridge, 1998).

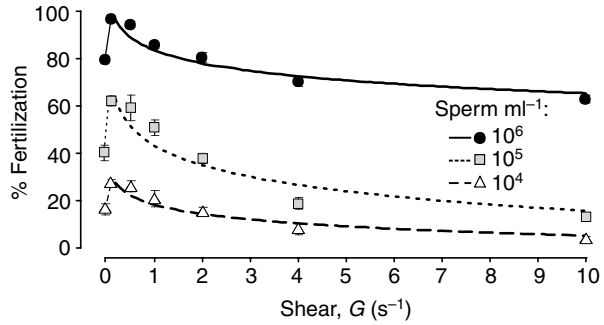

Fig. 4. Effects of fluid shear on fertilization success. Egg concentration was held constant (10^3 cells ml^{-1}), and three sperm concentrations were assayed in separate tests (see text for details). Fertilization is described as a function of log-shear, using least-squares regression to identify the best fits (10^6 sperm ml^{-1}: y=83–7$\log_{10}(x)$, r^2=0.76, $F_{1,83}$=166.1, P<0.001; 10^5 sperm ml^{-1}: y=42.6–12.2$\log_{10}(x)$, r^2=0.81, $F_{1,88}$=151.7, P<0.001; 10^4 sperm ml^{-1}: y=17.9–5.7$\log_{10}(x)$, r^2=0.80, $F_{1,87}$=157.7, P<0.001). Each symbol is a mean ± s.e.m.; error bars are smaller than symbol sizes in some cases.

Table 2. *Mean vector angles describing swimming behavior of live sperm near abalone eggs and brine shrimp eggs, and dead sperm transported passively in the vicinity of abalone eggs*

	Orientation θ (degrees)					
	Live sperm/abalone eggs		Live sperm/brine shrimp eggs		Dead sperm/live abalone eggs	
Shear (s^{-1})	Relative to egg	Relative to flow	Relative to egg	Relative to flow	Relative to egg	Relative to flow
0	5±23***	NA	147±170	NA	57±151	NA
0.1	3±2***	98±151	70±155	222±151	74±147	177±7***
0.5	6±11***	67±141	243±152	42±143	350±152	178±5***
1.0	6±19***	172±118	128±149	154±28**	16±142	178±7***
2.0	7±102	170±32*	76±142	178±21***	140±143	179±10***
4.0	123±141	177±19***	240±80	181±18***	292±137	179±7***
10.0	82±81	174±11***	229±135	189±10***	105±126	178±7***

Values are means ± s.e.m. ($N \geqslant 25$ for each treatment).

*$P<0.05$; **$P<0.01$; ***$P<0.001$; an asterisk denotes significantly directional swimming with respect to a defined origin, either flow or egg surface (V-test: $z>2.31$). NA, not applicable.

egg surface, but only in still water and at relatively low shears (0–1.0 s^{-1}) (ANOVA and Scheffé tests: $P<0.001$; see supplementary material Tables S2 and S3). Encounter rate, swim speed and orientation, and fertilization success each peaked at the lowest shear tested (0.1 s^{-1}), and decayed as shear increased (Table 2 and Figs 4, 6 and 7; ANOVA and Scheffé tests: $P<0.001$, see supplementary material Tables S1, S2, S3 and S4).

Control trials were conducted by substituting brine shrimp eggs for their abalone counterparts. Male gametes did not respond to the presence of these alternative eggs. In fact, abalone sperm moved at random with respect to the direction of a brine shrimp egg surface and swam at a slow constant speed, irregardless of the applied shear (Table 2 and Fig. 6A,C). As a consequence, gamete encounter rate declined significantly (ANOVA and Scheffé tests: $P<0.001$, see supplementary material Tables S5 and S6), but not to the level of dead sperm (Fig. 7).

Additional control trials, using abalone eggs and dead sperm, highlighted the influence of fluid shear and eliminated behavior as a confounding variable. The rates at which dead sperm encountered eggs were lower than those for all other treatments, but remained significantly elevated at low shears relative to still water (Fig. 7; ANOVA and Scheffé tests: $P<0.01$, see supplementary material Tables S7 and S8).

Shear effects on sperm orientation to flow were similar in the presence of brine shrimp eggs and abalone eggs. In both cases, the tendency of cells to swim downstream increased monotonically as a function of fluid shear (Fig. 6B). The slope was significantly higher, however, for sperm swimming among brine shrimp eggs (ANCOVA: $F_{1,8}=10.98$, $P=0.02$). This discrepancy likely resulted from faster swim speeds in the presence of abalone eggs that would more effectively oppose the flow (Fig. 6C).

Effects of fluid shear on sperm and egg rotation rates

When transported passively in a sheared flow, male and female gametes are predicted to exhibit either constant or periodic rotation, respectively (Bartok and Mason, 1957; Karp-Boss and Jumars, 1998). Egg and sperm rotation rates were evaluated relative to model predictions for spheres (eggs) and prolate spheroids (sperm) [see Eqn 6 (Jeffrey, 1922)]. For eggs,

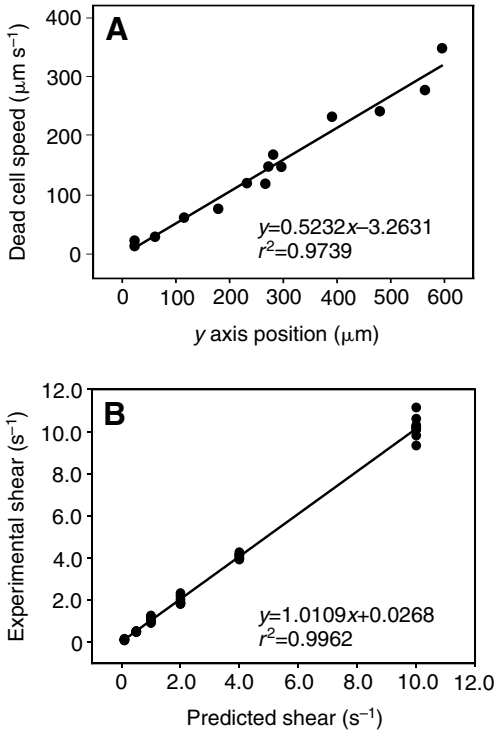

Fig. 5. Characterization of fluid shear across the gap within a Taylor-Couette flow tank. (A) Using dead sperm as passively transported particles, results are provided for a single trial at a predicted shear of 0.5 s^{-1} (see Eqn 1 and Eqn 2). Each data point is the speed of a single cell, plotted as a function of position along a cross-gap transect, beginning at the cross-over point of no translational velocity and running in a straight line towards the outer wall (perpendicular to the direction of fluid motion). The slope of the line is the fluid shear, and least-squares regression indicates an excellent fit of empirical and theoretical values (ANCOVA: $F_{1,12}=0.45$, $P=0.50$). (B) The entire data set for dead sperm trials ($N=60$), showing close agreement between predicted and experimental observations (ANCOVA: $F_{1,58}=0.01$, $P=0.92$).

empirical measurements and theoretical predictions were in excellent agreement (Fig. 8A; ANCOVA: $F_{1,57}<0.001$, $P>0.99$). As shear increased, female gametes rotated continuously and

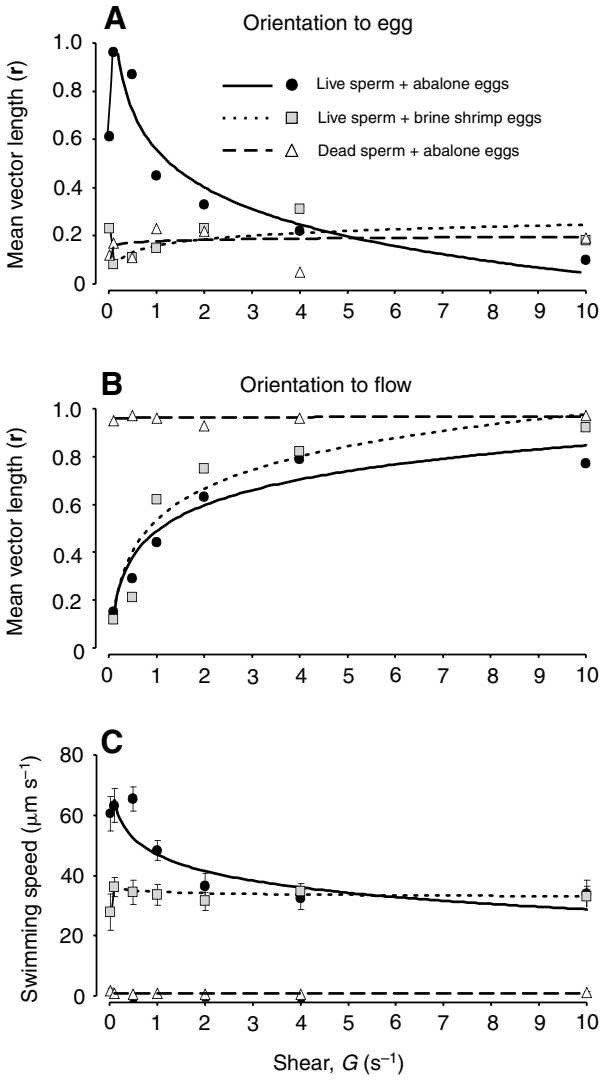

Fig. 6. Effects of fluid shear on sperm swim speed and direction. The mean direction of swimming is expressed in a circular coordinate system (see Table 2 and text for details). (A) Sperm swimming trajectory as evaluated with respect to the nearest egg surface. The unit vector length (**r**) is described as a function of log-shear, using least-squares regression to identify the best fits (live sperm, abalone eggs: y=–0.20log$_{10}$(x)+0.53, r^2=0.91, $F_{1,5}$=30.5, P<0.01; live sperm, brine shrimp eggs: y=0.03log$_{10}$(x)+0.16, r^2=0.53, $F_{1,5}$=4.63, P=0.10; dead sperm, abalone eggs: y=0.008log$_{10}$(x)+0.17, r^2=0.09, $F_{1,5}$=0.40, P=0.55). (B) Sperm swimming trajectory is evaluated as in A, but with the origin facing directly into flow (live sperm, abalone eggs: y=0.15log$_{10}$(x)+0.47, r^2=0.92, $F_{1,5}$=52.35, P<0.01; live sperm, brine shrimp eggs: y=0.19log$_{10}$(x)+0.52, r^2=0.90, $F_{1,5}$=36.26, P<0.01; dead sperm, abalone eggs: y=0.001log$_{10}$(x)+0.95, r^2=0.03, $F_{1,5}$=0.14, P=0.72). (C) Translational swimming speeds of sperm (live sperm, abalone eggs: y=47.6–7.8log$_{10}$(x), r^2=0.44, $F_{1,199}$=48.4, P<0.001; live sperm, brine shrimp eggs: y=34.–0.6log$_{10}$(x), r^2=0.04, $F_{1,119}$=0.44, P=0.49; dead sperm, abalone eggs: y=0.67–0.003log$_{10}$(x), r^2<0.01, $F_{1,118}$=0.004, P=0.95). Each symbol is a mean ± s.e.m.; error bars are smaller than symbol sizes in some cases.

with faster instantaneous velocities (Fig. 8A,B). Moreover, there was no effect of the jelly coat on egg rotation rate. The behavior of dead sperm, with their spheroid cell bodies forming an axis ratio of ~5, also conformed to the theoretical model. These cells tumbled, or rotated, at the expected rates (Fig. 9A; ANCOVA: $F_{1,57}$<0.001, P>0.99). Although live sperm did not tumble at lower shears, they began to rotate, much like dead cells, at 4.0 and 10.0 s^{-1} (one-way ANOVA: $F_{1,17}$=0.005, P=0.94). The transition in active sperm behavior to that of being passively transported and rotated was predicted based on the relationship between F_{swim} and F_{shear} (Fig. 9B). The theoretically derived threshold (F_{swim}/F_{shear}=1) was 2.0 s^{-1}, above which higher shears overwhelmed sperm swimming.

Effects of egg rotation on sperm-egg interactions

Egg rotation inhibited sperm contact, and hence, fertilization. Fluid speeds of 5.1, 25.3, 50.6 and 571 μm s^{-1} were generated at (<1 μm distant) rotating abalone egg surfaces in Taylor-Couette flows of 0.1, 0.5, 1.0 and 10.0 s^{-1}, respectively. In comparison, sperm swam at average speeds of 63.2, 65.5, 48.3 and 33.9 μm s^{-1} under these same flow conditions. Thus, sperm swimming could overcome advection at the abalone egg surface, but only in the two slowest flows. As fluid approached a rotating egg, fluid accelerated, streamlines compressed or closed, and shear stress increased locally near the surface facing into flow (Fig. 8B,C and Fig. 10A). Consequently, the likelihood of sperm 'slipping' around the egg surface, rather than encountering it, also rose significantly with rotation rate. In Taylor-Couette flows of 0.1 and 0.5 s^{-1}, the ratio of F_{swim}/F_{shear} was greater than unity at all points surrounding an egg, rotation effects were negligible, and male–female gamete encounter rates were maximal. When approaching from directly upstream, 74–80% of male gametes successfully attached to an egg. In contrast, sperm–egg encounter rates decreased significantly (ANOVA and Scheffé tests: P<0.001; see supplementary material Table S4) and only 59% of upstream sperm attached for a Taylor-Couette flow of 1.0 s^{-1}. Egg rotation contributed markedly to the local flow field. At G=1.0 s^{-1}, local shears as high as 2.5 s^{-1} occurred within 10 μm, and F_{swim}/F_{shear} was less than unity as far away as one sperm

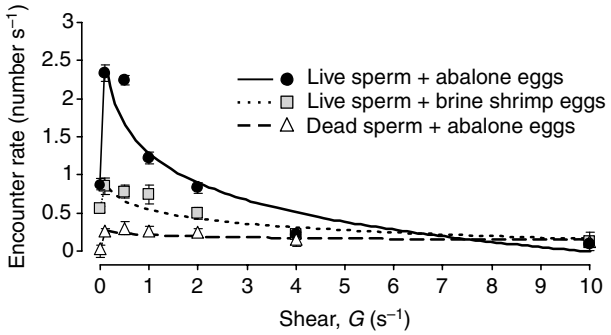

Fig. 7. Effects of fluid shear on sperm–egg encounter rate. Encounter rate is described as a function of log-shear, using least squares-regression to identify the best fits (live sperm, abalone eggs: y=1.29–0.56log$_{10}$(x), r^2=0.82, $F_{1,68}$=86.6, P<0.001; live sperm, brine shrimp eggs: y=0.55–0.16log$_{10}$(x), r^2=0.67, $F_{1,42}$=72.1, P<0.001; dead sperm, abalone eggs: y=0.22–0.29log$_{10}$(x), r^2=0.16, $F_{1,35}$=10.4, P<0.01). Each symbol is a mean ± s.e.m.; error bars are smaller than symbol sizes in some cases.

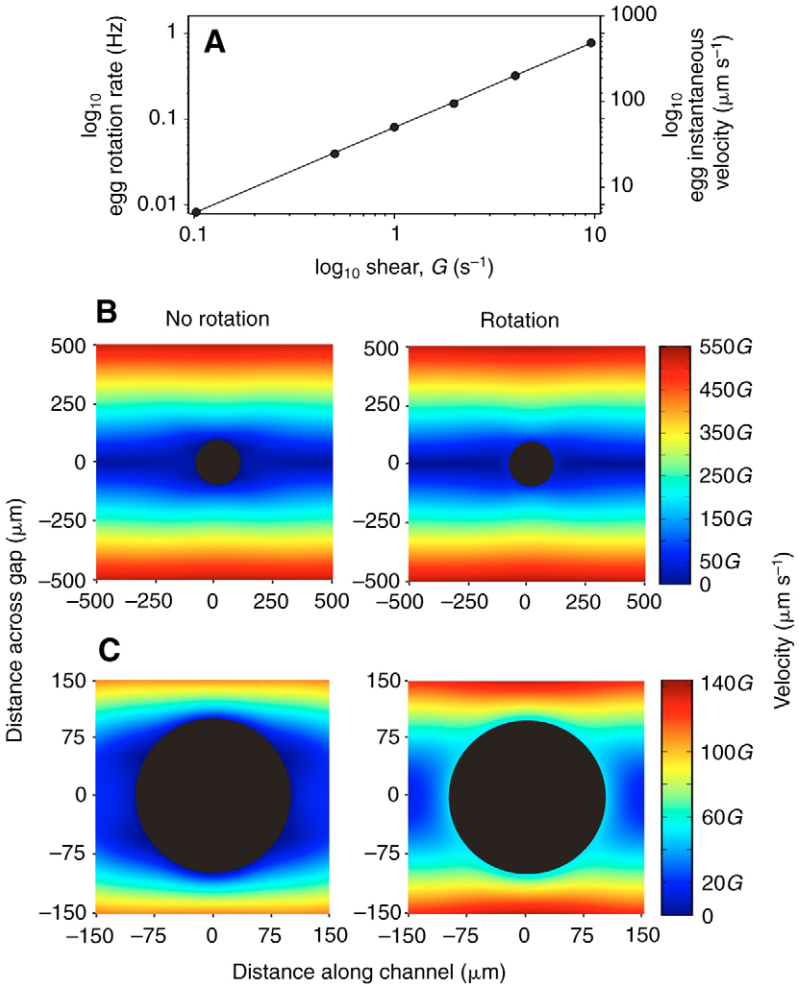

Fig. 8. (A) Abalone egg rotation rate and instantaneous rotational velocity as a function of fluid shear. The line is predicted from theory (see Eqn 6 and Eqn 7), and symbols (closed circles) are values obtained in experiments. Each symbol is a mean ± s.e.m.; error bars are smaller than symbol sizes in each case. (B) The flow fields surrounding an abalone egg, solved numerically (see Eqn 7 and Eqn 8) using the Navier–Stokes equation and the finite element method. Model outputs are displayed as velocity color maps for a non-rotating (Left) and rotating (Right) egg. The *x* and *y* axes are oriented parallel or perpendicular to the direction of flow, respectively. G (s^{-1}) is fluid shear generated in the Taylor-Couette flow tank. (C) Close-ups of flow fields shown in B.

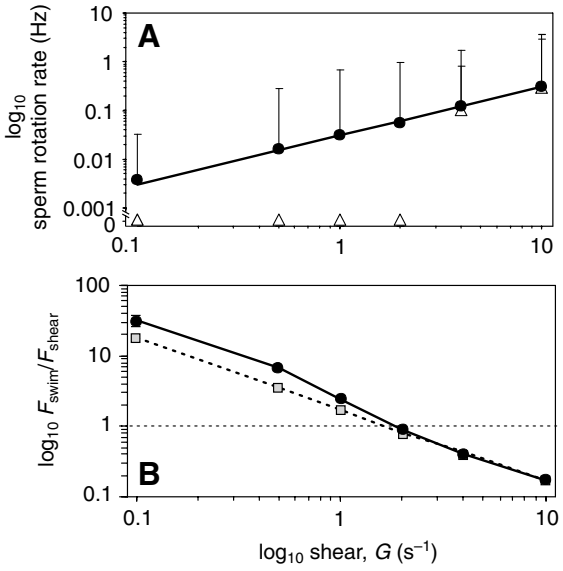

Fig. 9. (A) Abalone sperm rotation rate as a function of fluid shear, with male gametes modeled as prolate spheroids. The line is predicted from theory (see Eqn 6), and symbols are values obtained in experiments using dead (closed circles) or live (open triangles) cells. Each symbol is a mean + s.e.m.; error bars are smaller than symbols in some cases. (B) The relationship between F_{swim}/F_{shear} and fluid shear within the Taylor-Couette apparatus. F_{swim} was calculated using sperm swimming speeds in the presence of abalone (filled circles, solid line) or brine shrimp (filled squares, broken line) eggs.

length (~30 μm), of a rotating egg surface (Fig. 10B,C). Percentages dipped even further, to 43%, 29% and 12%, in Taylor-Couette flows of 2.0 s^{-1}, 4.0 s^{-1} and 10.0 s^{-1}, respectively.

Effects of fluid shear on gamete morphology and viability

Besides acting on sperm motility, shear might damage the flagellum, compromise the egg jelly layer or membrane, or weaken the vitality of male and/or female gametes. To investigate these possibilities, sperm and eggs were examined microscopically. Inspections showed no visible evidence for an influence of shear (at 0–10.0 s^{-1}) on egg size (radius), membrane or jelly coat (Table 3; ANOVA and Scheffé tests: $P>0.99$; see supplementary material Table S9; photomicrographs are available upon request). Sheared sperm were highly motile and possessed flagella of natural length. Moreover, no significant difference was found between swim speeds of male gametes before, or after, shearing (ANOVA and Scheffé tests: $P>0.76$; see supplementary material Table S10). When bioassays were performed subsequently in still water, the shearing of male and female gametes did not decrease fertilization success (Table 4; ANOVA and Scheffé tests: $P>0.36$; see supplementary material Tables S11 and S12). Combined results indicate no detrimental effects of shear on cell viability. Thus, findings of the Taylor-Couette experiments could be attributed solely to interactions between fluid dynamics and gamete behavior.

Discussion

As a consequence of their small sizes and relatively slow swimming speeds ($Re \ll 1$), the physical environment of sperm and eggs is dominated by viscous forces. The relationship between laminar-shear flow and cell motility therefore is a key determinant of fertilization success (Fauci and Dillon, 2006). At high shears, fluid forces effectively overwhelm sperm swimming, thereby inhibiting male–female gamete encounters, and hence fertilization. By inducing egg and sperm rotation, high shears also precipitate a decline in fertilization success. That is, a local increase in shear stress confers to sperm a heightened propensity to slip past an egg surface. Alternatively,

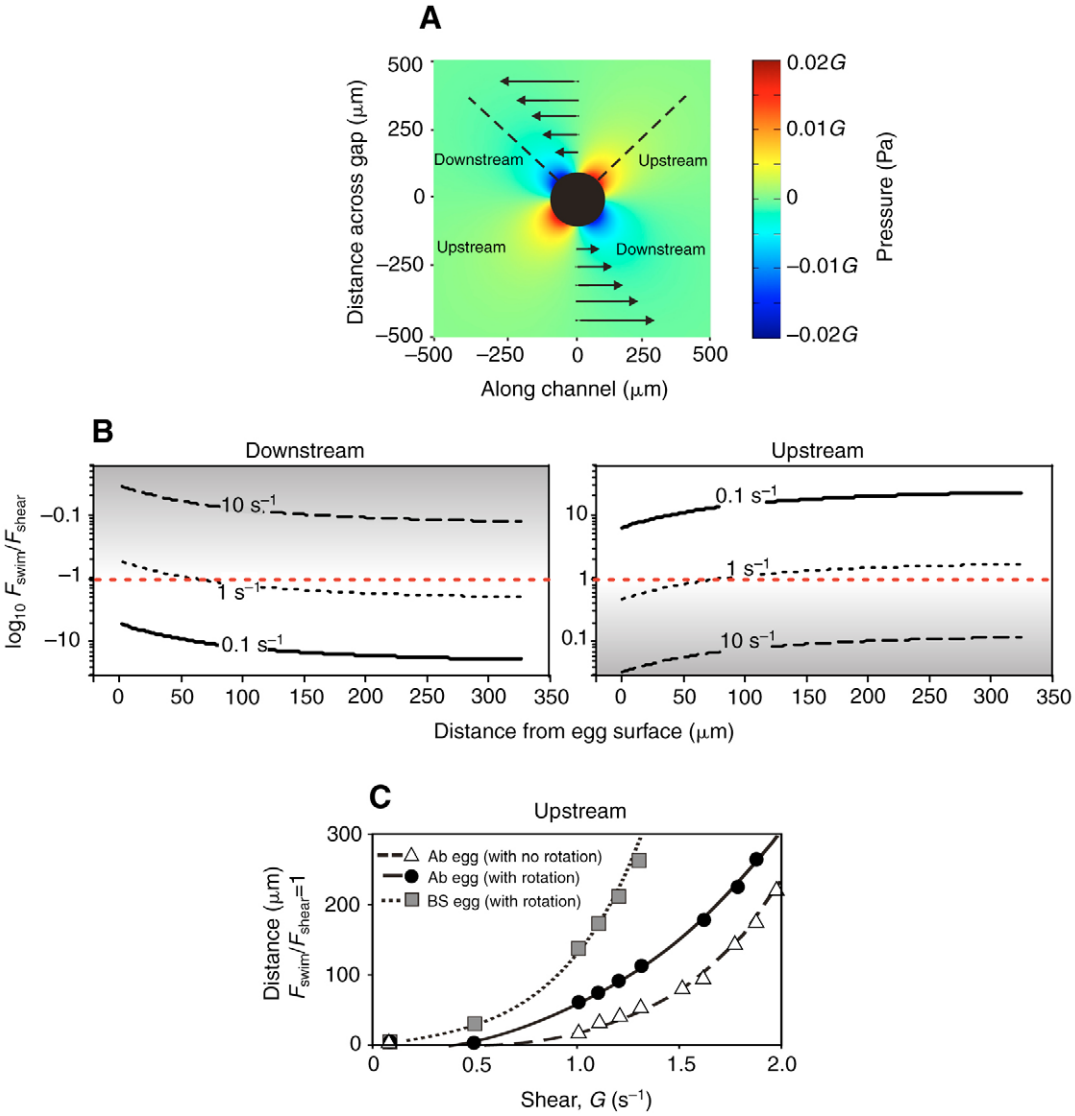

Fig. 10. (A) The shear stresses surrounding a rotating abalone egg. Model output is displayed as a pressure map, with *x* and *y* axes oriented parallel or perpendicular to the direction of flow, respectively. Relative to flow, two 45° transects (broken lines) were established upstream and downstream of the modeled egg surface. G (s^{-1}) is fluid shear generated in the Taylor-Couette flow tank. (B) The relationship between F_{swim}/F_{shear} and distance from the modeled egg surface along a downstream (Left) or upstream (Right) transect. Sperm were modeled as prolate spheroids. (C) Distance from the modeled egg surface along a upstream transect where $F_{swim}/F_{shear}=1$, as a function of G. Local shears vary substantially near an egg surface and are incorporated into our models. Three specific conditions were evaluated: an abalone (Ab) egg (with or without rotation) and a brine shrimp (BS) egg (with rotation).

low shears may promote fertilization by facilitating sperm navigation towards an egg. Thus, fluid shear conditions that constrain or conspire with gamete behavior would strongly predict fertilization success.

These relationships were quantified for red abalone *Haliotis rufescens*. Field studies identified meaningful properties of water motion within native microhabitats harboring adult populations of this species. Flow speeds and turbulent mixing were slow compared with adjacent, open, kelp forest environments. Previously, visual observations (using SCUBA) revealed that abalone spawn during calm sea states – slow ocean currents, small surface waves – and slack low or high water (Breen and Adkins, 1980; Stekoll and Shirley, 1993) (J.A.R. and R.K.Z., unpublished observations). Such tranquil flows minimize rates of gamete dilution by advection and turbulent mixing (Pearson et al., 1998; Marshall et al., 2004), and thus enhance fertilization success (Stekoll and Shirley, 1993). Fluid shears in laboratory experiments were scaled according to field-flow measurements. Sperm performed best and fertilization success was maximized under laboratory conditions most closely simulating the physical properties of adult microhabitats.

Fluid shear and sperm swimming

Cell motility conspires with fluid motion at low shears

Sperm actively recruited to conspecific eggs as a consequence of behavior. Relative to high shears, cells swam significantly faster and oriented more directly towards eggs at

Table 3. *Properties of sperm and eggs before and after shearing*

	Egg		Egg + jelly coat		Sperm					
	Radius (μm)		Radius (μm)		% motile		Swim speed (μm s^{-1})		% with flagella	
Shear (s^{-1})	Before	After	Before	After	Before	After	Before	After	Before	After
0	113.5±3.6	112.5±3.1	197.0±4.2	201.7±4.0	99.2±0.7	99.2±0.7	43.3±2.2	41.9±2.8	100.0	100.0
0.1	112.1±1.4	111.0±1.6	205.6±8.8	205.7±7.7	98.5±0.8	99.2±0.7	41.9±2.4	47.0±6.6	100.0	100.0
0.5	112.1±1.8	111.9±1.7	199.4±5.8	200.1±4.3	99.7±0.2	99.0±0.5	42.5±2.5	38.5±2.0	100.0	100.0
1.0	113.0±1.8	114.0±1.7	208.0±7.1	207.2±8.3	98.2±1.7	99.2±0.7	46.1±1.4	43.4±1.4	100.0	100.0
2.0	112.2±2.0	111.7±2.0	200.1±4.5	201.5±4.7	99.5±0.5	99.5±0.5	41.5±2.6	43.0±2.9	100.0	100.0
4.0	111.3±1.6	111.6±1.4	195.6±4.2	200.5±4.1	99.2±0.7	99.2±0.7	40.4±2.8	38.9±2.5	100.0	100.0
10.0	114.6±0.9	113.6±1.8	204.7±7.7	198.5±5.5	99.2±0.7	99.2±0.7	39.3±2.2	39.6±1.6	100.0	100.0

Values are means ± s.e.m. ($N \geqslant 10$ for each treatment).

low shears and in still water. A comparison between low shears and still water revealed that male gametes swam at the same speed under both conditions, but sperm navigation was significantly enhanced at low shears. Accordingly, fertilization success peaked in these slow flows.

The observed sperm behavior may be a product of both mechano- and chemo-sensory inputs. Dual transduction pathways for detecting chemical and mechanical stimuli have been well described for many cell types (Weber et al., 1999; Luu et al., 2000; Cinamon and Alon, 2003; Cuvelier and Patel, 2005). Mammalian white blood cells (eosinophils and leukocytes), for example, initiate locomotion and move upstream in response to a combination of fluid shear and a blood-borne chemical factor. The chemical and shear act as conditioning stimuli, but cells orient with respect to the mean direction of blood flow (Tranquillo et al., 1988; Rainger et al., 1999; Ley, 2003; Luu et al., 2003). Such behavior rapidly conveys them to inflamed tissues and invading microorganisms (Cinamon et al., 2004).

Like eosinophils and leukocytes (Tranquillo et al., 1988; Rainger et al., 1999; Ley, 2003; Luu et al., 2003), abalone sperm initiate faster locomotion in response to a waterborne chemical factor emitted by eggs. Unlike the white blood cells, however, sperm navigate with respect to a chemical concentration gradient even in the absence of flow (Riffell et al., 2002; Riffell et al., 2004). Consequently, sperm require chemical but not mechanical stimuli for directing locomotion. Low shear and slow flow conspire to create fluid-dynamic conditions that are highly conducive for broadcasting chemical signals (Zimmer and Butman, 2000). Egg attractant is released, and then transported by advection with minimal dilution. The result is a behaviorally active odor plume. Plume length and active volume peak at 0.1 s^{-1} and decay thereafter, reflecting precisely the patterns described for sperm recruitment and fertilization success (J.A.R. and R.K.Z., manuscript submitted for publication). Here, 'active volume' is defined by attractant concentrations above a behavioral threshold for chemotaxis induction (Riffell et al., 2002; Riffell et al., 2004).

Table 4. *Fertilization success of sperm and eggs before and after shearing*

	Egg		Sperm	
Shear (1 s^{-1})	Before	After	Before	After
0	86.0±1.8	86.9±2.9	84.5±3.5	86.9±2.4
0.1	89.7±4.1	87.5±1.9	89.5±2.3	87.2±2.3
0.5	88.2±1.5	86.0±2.4	86.2±2.4	85.0±3.3
1.0	88.7±2.7	87.0±2.7	85.4±2.3	87.7±3.2
2.0	85.2±1.6	87.2±1.8	89.2±1.1	89.7±2.2
4.0	87.5±1.8	84.2±1.9	86.7±2.0	88.7±2.2
10.0	88.2±1.3	87.0±1.7	87.0±1.7	87.5±3.6

Values are means ± s.e.m. (N=4 for each treatment).

Ultimately, sperm use a mechanism of helical klinotaxis to negotiate attractant gradients (Miller, 1985; Crenshaw, 1991; Crenshaw, 1996; Friedrich and Jülicher, 2007). When detecting a sufficient change in concentration over time, cells simultaneously arrest translational motion while increasing rotational velocity through an asymmetrical flagellar beat (Crenshaw, 1993; Babcock, 2003; Carlson et al., 2003; Qi et al., 2007). In an instant (<200 ms), these actions cause an abrupt turn, and thus, reorient the direction of sperm swimming (Miller and Brokaw, 1970; Yoshida et al., 2002; Yoshida et al., 2003; Spehr et al., 2004; Kaupp et al., 2006). Through fast, symmetrical flagellar beating, sperm finally move in a straight path towards the site of highest attractant concentration, an egg.

Fluid motion constrains cell motility at high shears

Changes in sperm behavior continued to develop beyond the threshold F_{swim}/F_{shear}=1. Because shear overwhelms motility, cells are unable to cross flow streamlines. Still, sperm swam at a reduced speed (30 μm s^{-1}) and oriented strongly with flow. These changes in sperm swimming at higher shears may be attributable to the hydrodynamic and viscous forces acting on the cell. Although sperm flagellar waveforms could not be identified from our digitized images, inferences were based on the kinematics of sperm paths. Helical paths were compressed (smaller amplitudes and frequencies) at relatively high shears. Evidently the sum of the forces acting on the cell body and flagellum restricted the rotation of wave propagation, thereby causing decreased flagellar amplitude and frequency and decay in swimming speed (Gray and Hancock, 1955; Reynolds, 1965; Chwang and Wu, 1971; Lighthill, 1975; Brennan and Winet, 1977). Sperm orientation also was influenced by strong fluid shear. To minimize drag, the rod-like shape of the cell body alone dictates sperm alignment, with the long axis orienting parallel to flow direction (Jeffrey, 1922; Goldsmith and Mason,

1962; Winet et al., 1984; Karp-Boss and Jumars, 1998; Karp-Boss et al., 2000). Yet, asymmetry in cell shape can cause male gametes to rotate at a rate predicted from Jeffrey's theory (Jeffrey, 1922) for prolate spheroids (Bretherton and Rothschild, 1961). In the present study, abalone sperm predominantly oriented with their heads facing downstream. Intermittent rotation and head orientation resulted from asymmetrical cell shape, combined with uneven distribution of mass (thereby imposing a gravitation torque) and stabilizing effects of the flagellum (Pedley and Kessler, 1992; Roberts and Deacon, 2002). Likewise, heat-killed bull sperm were aligned with heads facing downstream in response to laminar shear (Bretherton and Rothschild, 1961).

Fluid shear, sperm–egg encounter and fertilization success

Abalone gamete encounter rate and fertilization success were highly correlated, but nonlinearly related to shear. Most previous theoretical and empirical studies were conducted in still water. The probability of gamete encounter was parameterized as a function of sperm swimming speed, gamete concentration, and the 'target' area of an egg (Rothschild and Swann, 1951; Vogel et al., 1982; Levitan et al., 1991; Levitan, 2000). Given our results, still-water studies are unrealistic and cannot be extrapolated to dynamically scaled flows.

The nonlinearity we observed in gamete encounters and fertilization may be attributed to the following mechanisms. At low shears, cumulative effects of active cell behavior, such as chemotaxis, would enhance cell contacts and fertilization rate (Karp-Boss et al., 2000; Soghomonians et al., 2002; Smith et al., 2007). At high shears, near-cell (<20 μm) hydrodynamics induce gametes to rotate, and disassociate, thus accelerating a decline in gamete encounters and fertilization rate (Kiørboe and Titelman, 1998).

Attached sperm and egg would separate if sufficient shear force breaks the bond between them (Mohamed et al., 1999; Mohamed et al., 2000; Thomas et al., 2002). Abalone sperm and egg binding force is unknown, but for mammalian sperm and the zona pullicida, it was measured as 4×10^{-10}–3×10^{-9} N (Baltz et al., 1988; Thaler and Cardullo, 1996). Our numerical model yielded a maximal force on a rotating abalone egg surface of $<2\times10^{-11}$ N, well below the threshold for dissociating mammalian gametes. If the bond strength between gametes is similar among species, decay in abalone fertilization at high shears cannot be attributed to the forces dissociating sperm from egg. Instead, the mechanism involves a flow-driven decrease in gamete encounter rates as a consequence of reduced performance of swimming sperm.

The role of fluid dynamics in fertilization ecology

Dynamic scaling between field and laboratory flow environments provides an immediate ecological context for this study. Flows within the Taylor-Couette tank simulated the essential features of water motion in natural habitats where abalone sperm encounter eggs for the following reasons. First, highly one-dimensional currents provided the basic hydrodynamic setting. Turbulent fluctuations were 10–100 times higher along a principal (u) flow axis in abalone crevices and under ledges, similar to Taylor-Couette flow. Second, laminar shear characterized flow within the smallest eddies, sites of sperm swimming, egg rotation and fertilization. The Kolmogorov microscale, defining the tiniest eddy in the flow, was calculated as 0.6–1.7 mm [$\eta=(\upsilon^3/\epsilon)^{1/4}$], based on field measurements. Abalone egg diameters (including jelly coats) are 1.5–4 times smaller than these scales, indicating that eggs were, in fact, imbedded within a laminar shear flow regime (Tennekes and Lumley, 1972; Hinze, 1975). Third, turbulent fluctuations were essentially intermittent and scaled with gamete encounter time. From field data, the Kolmogorov scale for an eddy life time was 2–13 s [$\tau=2\pi(\upsilon/\epsilon)^{1/2}$], comparing favorably to the duration of our fertilization assays (15–30 s) (Riffell et al., 2004) (present study). Finally, flow steadiness was representative of the low frequency of turbulent bursts in the field. Near-instantaneous (30 Hz) bursts of turbulence produced shears (F_{shear}) exceeding sperm propulsion (F_{swim}) only ~16% of the time. Collectively, hydrodynamic conditions in laboratory experiments sufficiently simulated nature, allowing extrapolation of process from laboratory to field. Gamete behavior thus emerges as a critical determinant of sexual reproduction within natural abalone microhabitats.

For free-spawning organisms, fertilization is a two-step process where (1) male and female gamete clouds comingle, and (2) sperm contact and penetrate an egg. Contributions to fertilization success of larger (mixing of gamete plumes) and smaller (sperm–egg encounters) scale processes have yet to be isolated experimentally. The timing and sites chosen by adults when spawning, for example, might maximize simultaneously gamete cloud mixing and sperm-egg behavioral interactions. Alternatively, spawning events could promote cloud commingling over behavioral interactions, or *vice versa*, under sub-optimal environmental conditions. Knowledge of such compromises would provide critical insights into the relative importance and evolution of processes mediating fertilization at spawning *versus* gamete-interaction scales. Certain taxa (e.g. marine abalone and kelp, and terrestrial angiosperms), having diverse phylogenetic origins, release gametes into slow flows with reduced turbulent mixing (Whitehead, 1969; Serrão et al., 1996; Pearson et al., 1998; Culley et al., 2002). In these cases, either gamete behavior or adhesions between male and female sex cells at low shears play critical roles in fertilization. In contrast, other taxa (e.g. marine honeycomb worms and limpets) broadcast their gametes only under the extreme hydrodynamic conditions of winter storms, where length scales of the tiniest eddies are smaller than egg diameters (Lewis, 1986; Barry, 1989; Thomas, 1994). Fertilization occurs *via* gamete encounters due to passive physical transport; apparently, behavior is inconsequential.

When behavior matters, sperm motility of both internal and external fertilizers varies predictably among species (Chia et al., 1975; Hardy and Dent, 1986; Bakst, 1993; Simmons et al., 1999; Byrne et al., 2003). Sperm of internal fertilizers, for example, are subjected to fluid shears of 2–4 s^{-1} and 3–25 s^{-1} within the human uterus and Fallopian tubes, respectively (Blake et al., 1983; Winet et al., 1984; Eytan et al., 2001). Yet, sperm swimming is effective only in shears <4 s^{-1} (Bretherton and Rothschild, 1961; Winet et al., 1984). Consequently, fertilization in humans, like in abalone, involves active behaviors exploiting weak passive physical transport. In contrast, sperm of certain phylogenetically diverse internal and

external fertilizers are specifically adapted to negotiate high-shear flows; their long tails and streamlined bodies facilitate very fast swim speeds (Franzén, 1956; Hendelberg, 1986). Fluid shear, whether in a turbulent ocean or a human reproductive tract, thus acts as a decisive selective pressure driving the mechanics of sperm motility and gamete evolution.

This paper is dedicated to the memory of Mia J. Tegner, an ecologist and leading researcher for the preservation of endangered abalone species. We thank Kristin L. Riser and L. Ignacio Vilchis for providing assistance with field and laboratory tasks. Paul K. Dayton and Mike I. Latz graciously contributed ideas, laboratory space and facilities. Lee Karp-Boss and Peter A. Jumars provided helpful comments that greatly improved earlier drafts of the manuscript. Cheryl Ann Zimmer contributed to this project in every way possible, while Benjamin Beede, of The Cultured Abalone, Inc., kindly supplied animals and critical tips on husbandry. This work was supported by awards from the National Science Foundation (IBN 01-32635 and IBN 02-06775), California Sea Grant (Project R/F-197), the National Institutes of Health (2-K12-GM000708-06), and the UCLA Council on Research.

References

Adler, J. (1969). Chemoreceptors in bacteria. *Science* **166**, 1588-1597.

Adler, P. M. (1981). Heterocoagulation in shear flow. *J. Colloid Interface Sci.* **83**, 106-115.

Ameer, G. A., Barabino, G., Sasisekharan, R., Harmon, W., Cooney, C. L. and Langer, R. (1999). Ex vivo evaluation of a Taylor-Couette flow, immobilized heparinase I device for clinical application. *Proc. Natl. Acad. Sci. USA* **96**, 2350-2355.

Babcock, D. F. (2003). Development: smelling the roses? *Science* **299**, 1993-1994.

Babcock, R. and Keesing, J. (1999). Fertilization biology of the abalone *Haliotis laevigata*: laboratory and field studies. *Can. J. Fish. Aquat. Sci.* **56**, 1668-1678.

Bakst, M. R. (1994). Fate of fluorescent stained sperm following insemination: new light on oviducal sperm transport and storage in the turkey. *Biol. Reprod.* **50**, 987-992.

Baltz, J. M., Katz, D. F. and Cone, R. A. (1988). Mechanics of sperm-egg interaction at the zona pellucida. *Biophys. J.* **54**, 643-654.

Banse, K. (1982). Cell volumes, maximal growth rates of unicellular algae and ciliates, and the role of ciliates in the marine pelagial. *Limnol. Oceanogr.* **27**, 1059-1071.

Barry, J. T. (1989). Reproductive response of a marine annelid to winter storms: an analog to fire adaptation in plants? *Mar. Ecol. Progr. Ser.* **54**, 99-107.

Bartok, W. and Mason, S. G. (1957). Particle motions in sheared suspensions V. Rigid rods and collision of spheres. *J. Colloid Interface Sci.* **12**, 243-262.

Batschelet, E. (1981). *Circular Statistics in Biology*. New York: Academic Press.

Berg, H. C. (1983). *Random Walks in Biology*. Princeton: Princeton University Press.

Berg, H. C. and Purcell, E. M. (1977). The physics of chemoreception. *Biophys. J.* **20**, 193-219.

Blake, J. R., Vann, P. G. and Winet, H. (1983). A model of ovum transport. *J. Theor. Biol.* **102**, 145-166.

Breen, P. A. and Adkins, F. C. (1980). Spawning in British Columbia population of northern abalone *Haliotis kamtschatkana*. *Veliger* **23**, 177-179.

Brennan, C. and Winet, H. (1977). Fluid mechanics of propulsion by cilia and flagella. *Annu. Rev. Fluid Mech.* **9**, 339-498.

Bretherton, F. P. and Rothschild, L. (1961). Rheotaxis of spermatozoa. *Proc. R. Soc. Lond. B Biol. Sci.* **153**, 490-502.

Brooks, D. E. and Trust, T. J. (1983). Interactions of erythrocytes with bacteria under shear. *Ann. N. Y. Acad. Sci.* **416**, 319-331.

Byrne, P. G., Simmons, L. W. and Roberts, J. D. (2003). Sperm competition and the evolution of gamete morphology in frogs. *Proc. R. Soc. Lond. B Biol. Sci.* **270**, 2079-2086.

Carlson, A. E., Westenbroek, R. E., Quill, T., Ren, D., Clapham, D. E., Hille, B., Garbers, D. L. and Babcock, D. F. (2003). CatSper 1 required for evoked Ca^{2+} entry and control of flagellar function in sperm. *Proc. Natl. Acad. Sci. USA* **100**, 14864-14868.

Chen, X., Grey, J. Y., Thomas, S., Qiu, F., Medford, R. M., Wasserman, M. A. and Kunsch, C. (2004). Sphingosine kinase-1 mediates TNF-α-induced MCP-1 gene expression in endothelial cells: upregulation by oscillatory flow. *Am. J. Physiol.* **287**, H1452-H1458.

Chia, F. S., Atwood, D. and Crawford, B. (1975). Comparative morphology of echinoderm sperm and possible phylogenetic implications. *Am. Zool.* **15**, 533-565.

Chorin, A. J. (1994). *Vorticity and Turbulence*. New York: Springer.

Chwang, A. T. and Wu, T. Y. (1971). A note on the helical movement of micro-organisms. *Proc. R. Soc. Lond. B Biol. Sci.* **178**, 327-346.

Cinamon, G. and Alon, R. (2003). A real time in vitro assay for studying leukocyte transendothelial migration under physiological flow conditions. *J. Immunol. Methods* **273**, 53-62.

Cinamon, G., Shinder, V. and Alon, R. (2001). Shear forces promote lymphocyte migration across vascular endothelium bearing apical chemokines. *Nat. Immunol.* **2**, 515-522.

Cinamon, G., Shinder, V., Shamri, R. and Alon, R. (2004). Chemoattractant signals and b2 integrin occupancy at apical endothelial contacts combine with shear stress signals to promote transendothelial neutrophil migration. *J. Immunol.* **173**, 7282-7291.

Clarke, S. and Koshland, D. E. (1979). Membrane receptors for aspartate and serine in bacterial chemotaxis. *J. Biol. Chem.* **254**, 9695-9702.

Cox, K. W. (1962). California abalones, family Haliotidae. *Calif. Fish Game Fish. Bull.* **118**, 1-133.

Crenshaw, H. C. (1991). A technique for tracking spermatozoa in three dimensions without viscous wall effects. In *Comparative Spermatology: 20 Years After* (ed. B. Baccetti), pp. 353-357. New York: Raven Press.

Crenshaw, H. (1993). Orientation by helical motion III. Microrganisms can orient to stimuli by changing the direction of their rotational velocity. *Bull. Math. Biol.* **55**, 231-255.

Crenshaw, H. (1996). A new look at locomotion in microorganisms: rotating and translating. *Am. Zool.* **36**, 608-618.

Culley, T. M., Weller, S. G. and Sakai, A. K. (2002). The evolution of wind pollination in angiosperms. *Trends Ecol. Evol.* **17**, 361-369.

Cuvelier, S. L. and Patel, K. D. (2005). Studying leukocyte rolling and adhesion in vitro under flow conditions. *Methods Mol. Biol.* **290**, 331-342.

Daniels, R. and Floren, R. (1998). Poaching pressures in northern California's abalone fishery. *J. Shellfish Res.* **17**, 859-862.

Davis, G., Richards, D. V., Haaker, P. L. and Parker, D. O. (1992). Abalone population declines and fishery management in southern California. In *Abalone of the World: Biology, Fisheries and Culture* (ed. S. A. Guzman del Próo), pp. 237-249. Cambridge: Fishing News Books.

Dellimore, J. W. (1976). Conductimetric investigation of erythrocyte behaviour during shear flow of concentrated suspensions through a large tube. *Proc. R. Soc. Lond. B Biol. Sci.* **193**, 359-385.

Denny, M. W., Dairiki, J. and Distefano, S. (1992). Biological consequences of topography on wave-swept rocky shores: I. Enhancement of external fertilization. *Biol. Bull.* **183**, 220-232.

Denny, M. W., Nelson, E. K. and Mead, K. S. (2002). Revised estimates of the effects of turbulence on fertilization in the purple sea urchin, *Strongylocentrotus purpuratus*. *Biol. Bull.* **203**, 275-277.

Dickinson, R. B., Nagel, J. A., McDevitt, D., Foster, T. J., Proctor, R. A. and Cooper, S. L. (1995). Quantitative comparison of clumping factor- and coagulase-mediated *Staphylococcus aureus* adhesion to surface-bound fibrinogen under flow. *Infect. Immunol.* **63**, 3143-3150.

Dickinson, R. B., Nagel, J. A., Proctor, R. A. and Cooper, S. L. (1997). Quantitative comparison of shear-dependent *Staphylococcus aureus* adhesion to three polyurethane ionomer analogs with distinct surface properties. *J. Biomed. Mater. Res.* **36**, 152-162.

Dombrowski, C., Cisneros, L., Chatkaew, S., Goldstein, R. E. and Kessler, J. O. (2004). Self-concentration and large-scale coherence in bacterial dynamics. *Phys. Rev. Lett.* **93**, 1-4.

Ebert, E. E. (1992). Abalone aquaculture: a North American regional review. In *Abalone of the World: Biology, Fisheries and Culture* (ed. S. A. Shepherd, M. J. Tegner and S. A. Guzman del Próo), pp. 570-582. Oxford: Blackwell.

Edwards, N., Beeton, S., Bull, A. T. and Merchuk, J. C. (1989). A novel device for the assessment of shear effects on suspended microbial cultures. *Appl. Microbiol. Biotechnol.* **30**, 190-195.

Engelmann, T. W. (1883). *Bacterium photometricum*. Ein betrag zur vergleichenden physiologie des licht-und farbensinnes. *Arch. Physiol.* **30**, 95-124.

Eytan, O., Jaffa, A. J. and Elad, D. (2001). Peristaltic flow in a tapered channel: application to embryo transport within the uterine cavity. *Med. Eng. Phys.* **23**, 473-482.

Fauci, L. J. and Dillon, R. (2006). Biofluidmechanics of reproduction. *Annu. Rev. Fluid Mech.* **38**, 371-394.
Franzén, A. (1956). On spermiogenesis, morphology of the spermatozoon, and biology of fertilization among invertebrates. *Zool. Bidrag. Uppsala* **31**, 355-482.
Friedlich, B. M. and Jülicher, F. (2007). Chemotaxis of sperm cells. *Proc. Natl. Acad. Sci. USA* **104**, 13256-13261.
Fulford, G. R., Katz, D. F. and Powell, R. L. (1998). Swimming of spermatozoa in a linear viscoelastic fluid. *Biorheology* **35**, 295-309.
Gargett, A. E. (1989). Ocean turbulence. *Annu. Rev. Fluid Mech.* **21**, 419-511.
Gee, C. C. and Zimmer-Faust, R. K. (1997). Effects of walls, paternity and aging on sperm motility. *J. Exp. Biol.* **200**, 3185-3192.
Girard, P. and Nerem, R. (1995). Shear stress modulates endothelial cell morphology and F-actin organization through the regulation of focal adhesion-associated proteins. *J. Cell. Physiol.* **163**, 179-193.
Goldsmith, H. L. and Marlow, J. (1972). Flow behavior of erythrocytes. I. Rotation and deformation in dilute suspensions. *Proc. R. Soc. Lond. B Biol. Sci.* **182**, 351-384.
Goldsmith, H. L. and Mason, S. G. (1962). Particle motions in sheared suspensions XIII. The spin and rotation of disks. *J. Fluid Mech.* **12**, 88-96.
Goldsmith, H. L. and Turitto, V. T. (1986). Rheological aspects of thrombosis and haemostasis: basic principles and applications. *Thromb. Haemost.* **55**, 415-422.
Goldsmith, H. L., Quinn, T. A., Drury, G., Spanos, C., McIntosh, F. A. and Simon, S. I. (2001). Dynamics of neutrophil aggregation in Couette flow revealed by videomicroscopy: effect of shear rate on two-body collision efficiency and doublet lifetime. *Biophys. J.* **81**, 2020-2034.
Gray, J. and Hancock, G. J. (1955). The propulsion of sea-urchin spermatozoa. *J. Exp. Biol.* **32**, 802-814.
Gross, T. F. and Nowell, A. R. M. (1983). Mean flow and turbulence scaling in a tidal boundary layer. *Cont. Shelf Res.* **2**, 109-206.
Hahn, K. O. (1989). *Handbook of Culture of Abalone and Other Marine Gastropods*. Boca Raton, FL: CRC Press.
Happel, J. and Brenner, H. (1965). *Low Reynolds Number Hydrodynamics*. Englewood Cliffs, NJ: Prentice-Hall.
Hardy, M. P. and Dent, J. N. (1986). Transport of sperm within the cloaca of the female red-spotted newt. *J. Morphol.* **190**, 259-270.
Heathershaw, A. D. and Simpson, J. H. (1978). The sampling variability of the Reynolds stress and its relation to boundary shear stress and drag coefficient measurements. *Estuar. Coast. Shelf Sci.* **6**, 263-274.
Hendelberg, J. (1986). The phylogenetic significance of sperm morphology in the Platyhelminthes. *Hydrobiologia* **132**, 53-58.
Highgate, D. J. and Whorlow, R. W. (1970). Rheological properties of suspensions of spheres in non-Newtonian media. *Rheol. Acta* **9**, 569-576.
Hinze, J. O. (1975). *Turbulence; An Introduction to its Mechanism and Theory*. New York: McGraw Hill.
Hjelmfelt, A. T. and Mokros, L. F. (1966). Motion of discrete particles in a turbulent fluid. *Appl. Sci. Res.* **16**, 149-161.
Jannasch, H. W., Nelson, D. C. and Wirsen, C. O. (1989). Massive natural occurrence of unusually large bacteria (*Beggiatoa* sp.) at a hydrothermal deep-sea vent site. *Nature* **342**, 834-836.
Jeffrey, G. B. (1922). The motion of ellipsoidal particles immersed in a viscous fluid. *Proc. R. Soc. Lond.* **102**, 161-179.
Jeon, N. L., Baskaran, H., Dertinger, S. K. W., Whitesides, G. M., Van de Water, L. and Toner, M. (2002). Neutrophil chemotaxis in linear and complex gradients of interleukin-8 formed in a microfabricated device. *Nat. Biotechnol.* **20**, 826-830.
Kadash, K. E., Lawrence, M. B. and Diamond, S. L. (2004). Neutrophil string formation: hydrodynamic thresholding and cellular deformation during cell collisions. *Biophys. J.* **86**, 4030-4039.
Karp-Boss, L. and Jumars, P. A. (1998). Motion of diatom chains in steady shear flow. *Limnol. Oceanogr.* **43**, 1767-1773.
Karp-Boss, L., Boss, E. and Jumars, P. A. (1996). Nutrient fluxes to planktonic osmotrophs in the presence of fluid motion. *Oceanogr. Mar. Biol. Annu. Rev.* **34**, 71-107.
Karp-Boss, L., Boss, E. and Jumars, P. A. (2000). Motion of dinoflagellates in a simple shear flow. *Limnol. Oceanogr.* **45**, 1594-1602.
Katz, D. F., Bloom, T. D. and BonDurant, R. H. (1981). Movement of bull spermatozoa in cervical mucus. *Biol. Reprod.* **25**, 931-937.
Kaupp, U. B., Hildebrand, E. and Weyand, I. (2006). Sperm chemotaxis in marine invertebrates – molecules and mechanisms. *J. Cell. Physiol.* **208**, 487-496.
Kiørboe, T. and Titelman, J. (1998). Feeding, prey selection and prey encounter mechanisms in the heterotrophic dinoflagellate *Noctiluca scintillans*. *J. Plankton Res.* **20**, 1615-1636.
Konstantopoulos, K., Kukreti, S. and McIntire, L. V. (1998). Biomechanics of cell interactions in shear fields. *Adv. Drug Deliv. Rev.* **33**, 141-164.
Kundu, P. K. (1990). *Fluid Mechanics*. New York: Academic Press.
Leighton, D. L. (1989). Abalone (Genus *Haliotis*) mariculture on the North American Pacific coast. *Fish. Bull.* **87**, 689-702.
Leighton, D. L. (2000). *The Biology and Culture of the California Abalone*. Pittsburg: Dorrance Publishing.
Levitan, D. R. (1998). Does Bateman's principle apply to broadcast-spawning organisms? Egg traits influence *in situ* fertilization rates among congeneric sea urchins. *Evolution* **52**, 1043-1056.
Levitan, D. R. (2000). Sperm velocity and longevity trade off each other and influence fertilization in the sea urchin *Lytechinus variegates*. *Proc. R. Soc. Lond. B Biol. Sci.* **267**, 531-534.
Levitan, D. R., Sewell, M. A. and Chia, F. S. (1991). Kinetics of fertilization in the sea urchin *Strongylocentrotus franciscanus*: interaction of gamete dilution, age and contact time. *Biol. Bull.* **181**, 371-378.
Lewis, J. R. (1986). Latitudinal trends in reproduction, recruitment and population characteristics of some rocky littoral molluscs and cirripedes. *Hydrobiologia* **142**, 1-13.
Ley, K. (2003). Arrest chemokines. *Microcirculation* **10**, 289-295.
Li, Z. S., Mohamed, N. and Ross, J. M. (2000). Shear stress affects the kinetics of *Staphylococcus aureus* adhesion to collagen. *Biotechnol. Prog.* **16**, 1086-1090.
Lighthill, J. (1975). *Mathematical Biofluiddynamics*. Philadelphia: Society for Industry and Applied Mechanics.
Logan, E. L. and Kirchman, D. L. (1991). Uptake of dissolved organics by marine bacteria as a function of fluid motion. *Mar. Biol.* **111**, 175-181.
Luu, N. T., Rainger, G. E. and Nash, G. B. (2000). Differential ability of exogenous chemotactic agents to disrupt transendothelial migration of flowing neutrophils. *J. Immunol.* **164**, 5961-5969.
Luu, N. T., Rainger, G. E., Buckley, C. D. and Nash, G. B. (2003). CD31 regulates direction and rate of neutrophil migration over and under endothelial cells. *J. Vasc. Res.* **40**, 467-479.
Marshall, D. J., Semmens, D. and Cook, C. (2004). Consequences of spawning at low tide: limited gamete dispersal for a rock-pool anemone. *Mar. Ecol. Prog. Ser.* **266**, 135-142.
McCue, S., Noria, S. and Langille, B. L. (2004). Shear-induced reorganization of endothelial cell cytoskeleton and adhesion complexes. *Trends Cardiovasc. Med.* **14**, 143-151.
Mead, K. S. and Denny, M. W. (1995). The effects of hydrodynamic shear stress on fertilization and early development of the purple sea urchin *Strongylocentrotus purpuratus*. *Biol. Bull.* **188**, 46-56.
Meng, Y., Li, Y., Galvani, C. D., Hao, G., Turner, J. N., Burr, T. J. and Hoch, H. C. (2005). Upstream migration of *Xylella fastidiosa* via pilus-driven twitching motility. *J. Bacteriol.* **187**, 5560-5567.
Miller, R. L. (1979). Sperm chemotaxis in the hydromedusae. I. Species specificity and sperm behavior. *Mar. Biol.* **53**, 99-114.
Miller, R. L. (1985). Demonstration of sperm chemotaxis in Echinodermata: Asteroidea, Holothuroidea, Ophiuroidea. *J. Exp. Zool.* **234**, 383-414.
Miller, R. L. and Brokaw, C. J. (1970). Chemotactic turning behavior of *Tubularia* spermatozoa. *J. Exp. Biol.* **52**, 699-706.
Mohamed, N., Teeters, M. A., Patti, J. M., Höök, M. and Ross, J. M. (1999). Inhibition of *Staphylococcus aureus* adherence to collagen under dynamic conditions. *Infect. Immunol.* **67**, 589-594.
Mohamed, N., Rainier, T. R. and Ross, J. M. (2000). A novel experimental study of receptor-mediated bacterial adhesion under the influence of fluid shear. *Biotechnol. Bioeng.* **68**, 628-636.
Morse, D. E., Duncan, H., Hooker, N. and Morse, A. (1977). Hydrogen peroxide induces spawning in mollusks, with activation of prostaglandin endoperoxide synthetase. *Science* **196**, 298-300.
Mottett, M. G. (1978). A review of the fishery biology of abalones. *Wash. Dept. Fish. Tech. Rep.* **37**, 1-78.
O'Brien, K. R., Meyer, D. L., Waite, A. M., Ivey, G. N. and Hamilton, D. P. (2004). Disaggregation of *Microcystis aeruginosa* colonies under turbulent mixing: laboratory experiments in a grid-stirred tank. *Hydrobiologia* **519**, 143-152.
Packer, H. L. and Armitage, J. P. (1993). The unidirectional flagellar motor of *Rhodobacter sphaeroides* WS8 can rotate either clockwise or counterclockwise: characterization of the flagellum under both conditions by antibody decoration. *J. Bacteriol.* **175**, 6041-6045.
Pearson, G. A., Serrão, E. A. and Brawley, S. H. (1998). Control of gamete release in fucoid algae: sensing hydrodynamic conditions via carbon acquisition. *Ecology* **79**, 1725-1739.
Pedley, T. J. and Kessler, J. O. (1992). Hydrodynamic phenomena in suspensions of swimming microorganisms. *Annu. Rev. Fluid Mech.* **24**, 313-358.
Pennington, J. T. (1985). The ecology of fertilization in echinoid eggs: the consequences of sperm dilution, adult aggregation, and synchronous spawning. *Biol. Bull.* **169**, 417-430.

Pepper, D. W. and Heinrich, J. C. (2005). *The Finite Element Method: Basic Concepts and Applications*. Philadelphia: Hemisphere Publishing.

Qi, H., Moran, M. M., Navarro, B., Chong, J. A., Krapivinsky, G., Krapivinsky, L., Kirichok, Y., Ramsey, I. S., Quill, T. A. and Clapham, D. E. (2007). All four CatSper ion channel proteins are required for male fertility and sperm cell hyperactivated motility. *Proc. Natl. Acad. Sci. USA* **104**, 1219-1223.

Rainger, G. E., Buckley, C. D., Simmons, D. L. and Nash, G. B. (1999). Neutrophils sense flow-generated stress and direct their migration through alphaVbeta3-integrin. *Am. J. Physiol*. **276**, H858-H864.

Reynolds, A. J. (1965). The swimming of minute organisms. *J. Fluid Mech.* **23**, 241-260.

Riffell, J. A., Krug, P. J. and Zimmer, R. K. (2002). Fertilization in the sea: the chemical identity of an abalone sperm attractant. *J. Exp. Biol.* **205**, 1439-1450.

Riffell, J. A., Krug, P. J. and Zimmer, R. K. (2004). The ecological and evolutionary consequences of sperm chemoattraction. *Proc. Natl. Acad. Sci. USA* **101**, 4501-4506.

Roberts, A. M. and Deacon, F. M. (2002). Gravitaxis in motile micro-organisms: the role of fore-aft body asymmetry. *J. Fluid Mech*. **452**, 405-423.

Rossman, I. (1937). Uterine contractions and the transport of sperm in the rat. *Anat. Rec.* **69**, 133-149.

Rothschild, B. J. and Osborn, T. R. (1988). Small-scale turbulence and plankton contact rates. *J. Plankton Res.* **10**, 465-474.

Rothschild, L. and Swann, M. M. (1951). The fertilization reaction in the sea urchin: the probability of a successful sperm–egg collision. *J. Exp. Biol.* **28**, 403-416.

Serrão, E. A., Pearson, G. A., Kautsky, L. and Brawley, S. H. (1996). Successful external fertilization in turbulent environments. *Proc. Natl. Acad. Sci. USA* **93**, 5286-5290.

Shimeta, J. and Jumars, P. A. (1991). Physical mechanisms and rates of particle capture by suspension-feeders. *Oceanogr. Mar. Biol. Annu. Rev.* **29**, 191-257.

Shimeta, J., Jumars, P. A. and Lessard, E. J. (1995). Influences of turbulence on suspension feeding by planktonic protozoa: experiments in laminar shear fields. *Limnol. Oceanogr.* **40**, 845-859.

Shiu, Y. T., Li, S., Marganski, W. A., Usami, S., Schwartz, M. A., Wang, Y. L., Dembo, M. and Chien, S. (2004). Rho mediates the shear-enhancement of endothelial cell migration and traction force generation. *Biophys. J.* **86**, 2558-2565.

Short, M. B., Solari, C. A., Ganguly, S., Powers, T. R., Kessler, J. O. and Goldstein, R. E. (2006). Flows driven by flagella of multicellular organisms enhance long-range molecular transport. *Proc. Natl. Acad. Sci. USA* **103**, 8315-8319.

Simmons, L. W., Parker, G. A. and Stockley, P. (1999). Sperm displacement in the yellow dung fly, *Scatophaga stercoraria*: an investigation of male and female processes. *Am. Nat.* **153**, 302-314.

Smith, L. A., Aranda-Espinoza, H., Haun, J. B. and Hammery, D. A. (2007). Interplay between shear stress and adhesion on neutrophil locomotion. *Biophys. J.* **92**, 632-640.

Soghomonians, A., Barakat, A. I., Thirkill, T. L., Blankenship, T. N. and Douglas, G. C. (2002). Effect of shear stress on migration and integrin expression in macaque trophoblast cells. *Biochim. Biophys. Acta* **1589**, 233-246.

Solomon, M. J. and Boger, D. V. (1998). The rheology of aqueous dispersions of spindle-type colloidal hematite rods. *J. Rheol.* **42**, 929-949.

Spehr, M., Schwane, K., Riffell, J. A., Barbour, J., Zimmer, R. K. and Hatt, H. (2004). Particulate adenylate cyclase plays a key role in human sperm olfactory receptor-mediated chemotaxis. *J. Biol. Chem.* **279**, 40194-40203.

Stekoll, M. S. and Shirley, T. C. (1993). In situ spawning behavior of an Alaskan population of pinto abalone, *Haliotis kamtschatkana* Jonas, 1845. *Veliger* **36**, 95-96.

Tegner, M. J. (1989). The California abalone fishery: production, ecological interactions, and prospects for the future. In *Marine Invertebrate Fisheries: Their Assessment and Management* (ed. J. F. Caddy), pp. 401-420. New York: John Wiley and Sons.

Tegner, M. J. (2000). Abalone (*Haliotis* spp.) enhancement in California: what we've learned and where we go from here. *Can. Spec. Publ. Fish. Aquat. Sci.* **130**, 61-71.

Tennekes, H. and Lumley, J. (1972). *A First Course in Turbulence*. Cambridge: The MIT Press.

Thaler, C. D. and Cardullo, R. A. (1996). The initial molecular interaction between mouse sperm and the zona pellucida is a complex binding event. *J. Biol. Chem.* **271**, 23289-23297.

Thomas, F. I. M. (1994). Transport and mixing of gametes in three free-spawning polychaete annelids, *Phragmatopoma californica* (Fewkes), *Sabellaria cementarium* (Moore), and *Schizobranchis insignis* (Bush). *J. Exp. Mar. Biol. Ecol.* **179**, 11-27.

Thomas, W. E., Trintchina, E., Forero, M., Vogel, V. and Sokurenko, E. V. (2002). Bacterial adhesion to target cells enhanced by shear force. *Cell* **109**, 913-923.

Tranquillo, R. T., Zigmond, S. H. and Lauffenburger, D. A. (1988). Measurement of the chemotaxis coefficient for human neutrophils in the under-agarose migration assay. *Cell Motil. Cytoskel.* **11**, 1-15.

Trevelyan, B. J. and Mason, S. G. (1951). Particle motions in sheared suspensions. I. Rotations. *J. Colloid Interface Sci.* **6**, 354-367.

Trowbridge, J. H. (1998). On a technique for direct measurement of turbulent Reynolds stress in the presence of surface waves. *J. Atmos. Oceanic Technol.* **15**, 290-298.

Tutschulte, T. C. (1976). The comparative ecology of three sympatric abalone. PhD Dissertation, University of California, Santa Barbara, USA.

Tutschulte, T. and Connell, J. H. (1988). Growth of three species of abalones (*Haliotis*) in southern California. *Veliger* **31**, 204-213.

Tuval, I., Cisneros, L., Dombrowski, C., Wolgemuth, C. W., Kessler, J. O. and Goldstein, R. E. (2005). Bacterial swimming and oxygen transport near contact lines. *Proc. Natl. Acad. Sci. USA* **102**, 2277-2282.

Vacquier, V. D. (1998). Evolution of gamete recognition proteins. *Science* **281**, 1995-1998.

Verfürth, R. (1996). *A Review of a posteriori Error Estimation and Adaptive Mesh-renement Techniques.* Stuttgart: Wiley-Teubner.

Vilchis, L. I., Tegner, M. J., Moore, J. D., Friedman, C. S., Riser, K. L., Robbins, T. T. and Dayton, P. K. (2005). Ocean warming effects on growth, reproduction, and survivorship of southern California abalone. *Ecol. Appl.* **15**, 469-480.

Vogel, H., Czihak, G., Chang, P. and Wolf, W. (1982). Fertilization kinetics of sea urchin eggs. *Math. Biosci.* **58**, 189-216.

Weber, K. S., von Hundelshausen, P., Clark-Lewis, I., Weber, P. C. and Weber, C. (1999). Differential immobilization and hierarchical involvement of chemokines in monocyte arrest and transmigration on inflamed endothelium in shear flow. *Eur. J. Immunol.* **29**, 700-712.

Wesson, J. C. and Gregg, M. C. (1994). Mixing at Camarinal Sill in the Strait of Gibraltar. *J. Geophys. Res.* **99**, 9847-9878.

West, G. B., Brown, J. H. and Enquist, B. J. (1997). A general model for the origin of allometric scaling laws in biology. *Science* **276**, 122-126.

Whitehead, D. R. (1969). Wind pollination in the angiosperms: evolutionary and environmental considerations. *Evolution* **23**, 28-35.

Winet, H., Bernstein, G. S. and Head, J. (1984). Observations on the response of human spermatozoa to gravity, boundaries and fluid shear. *J. Reprod. Fertil.* **70**, 511-523.

Yoshida, M., Murata, M., Inaba, K. and Morisawa, M. (2002). A chemoattractant for ascidian spermatozoa is a sulfated steroid. *Proc. Natl. Acad. Sci. USA* **99**, 14831-14836.

Yoshida, M., Ishikawa, M., Izumi, H., Santis, R. and Morisawa, M. (2003). Store-operated calcium channel regulates the chemotactic behavior of ascidian sperm. *Proc. Natl. Acad. Sci. USA* **100**, 149-154.

Young, J. S. and DeMartini, J. D. (1970). The reproductive cycle, gonadal histology and gametogenesis of the red abalone, *Haliotis rufescens*. *Calif. Fish Game* **56**, 298-309.

Zimmer, R. K. and Butman, C. A. (2000). Chemical signaling processes in the marine environment. *Biol. Bull.* **198**, 168-187.

Zimmerman, W. B. (2004). *Process Modeling and Simulation with Finite Element Methods.* Singapore: World Scientific Publishing.

Zirbel, M. J., Veron, F. and Latz, M. I. (2000). The reversible effect of flow on the morphology of *Ceratocorys horrida* (Peridiniales, Dinophyta). *J. Phycol.* **36**, 46-58.